0090-9556/09/3707-1378–1394$20.00
DRUG METABOLISM AND DISPOSITION
Vol. 37, No. 7
25742/3484161
DMD 37:1378–1394, 2009
Printed in U.S.A.

In Vitro Metabolism of the Novel, Highly Selective Oral Angiogenesis Inhibitor Motesanib Diphosphate in Preclinical Species and in Humans

Chun Li,[1] Mita Kuchimanchi, Dean Hickman, Leszek Poppe, Mike Hayashi, Yihong Zhou, Raju Subramanian, Gondi Kumar,[2] and Sekhar Surapaneni[2]

Department of Pharmacokinetics and Drug Metabolism (C.L., M.K., D.H., M.H., Y.Z., R.S., G.K., S.S.) and Department of Molecular Structure (L.P.), Amgen Inc., Thousand Oaks, California

Received November 19, 2008; accepted April 13, 2009

ABSTRACT:

Motesanib diphosphate is a novel, investigational, highly selective oral inhibitor of the receptor tyrosine kinases vascular endothelial growth factor receptors 1, 2, and 3, the platelet-derived growth factor receptor, and the stem cell factor receptor (Kit). The in vitro metabolic profiles of [^{14}C]motesanib were examined by using microsomes and hepatocytes from preclinical species and humans. Several oxidative metabolites were observed and characterized by tandem mass spectrometry, nuclear magnetic resonance spectroscopy, and coinjection with authentic standards. Cytochrome P450 (P450) 3A4 is the major isozyme involved in the oxidative biotransformation of motesanib, but the CYP2D6 and CYP1A isozymes also make minor contributions. In hepatocyte incubations, oxidative and conjugative pathways were observed for all species examined, and indoline *N*-glucuronidation was the dominant pathway. Three less common and novel phase II conjugates of the indoline nitrogen were detected in hepatocytes and in microsomes supplemented with specific cofactors, including *N*-carbamoyl glucuronide, *N*-glucose, and *N*-linked *β*-*N*-acetylglucosamine. An *N*-glucuronide metabolite was the most frequently observed phase II conjugate in liver microsomes of all species, whereas the *N*-acetylglucosamine conjugate was observed only in monkey liver microsomes. Incubations with recombinant human UDP-glucuronosyltransferases (UGTs) and inhibition by the UGT1A4 and UGT1A1 substrates/inhibitors imipramine and bilirubin suggested that UGT1A4 is the major UGT isozyme catalyzing the *N*-glucuronidation of motesanib, with a minor contribution from UGT1A1. The in vitro metabolic profiles were similar between the human and preclinical species examined. All metabolites found in humans were also detected in other species.

Motesanib diphosphate (formerly known as AMG 706) (Fig. 1) is a highly selective kinase inhibitor with both antiangiogenic and direct antitumor activity (Polverino et al., 2006; Rosen et al., 2007). Motesanib is an ATP-competitive inhibitor of vascular endothelial growth factor (VEGF) receptors 1, 2, and 3, platelet-derived growth factor (PDGF) receptor, and stem cell factor receptor (Kit), which have all been implicated in the pathogenesis of human tumors (Dvorak, 2002; Heinrich et al., 2002; Song et al., 2005). In preclinical models of human cancer, oral administration of motesanib potently inhibited VEGF-induced angiogenesis in the rat corneal model and induced regression of established A431 xenografts (Polverino et al., 2006). Furthermore, motesanib has shown antiangiogenic and antitumor activity in patients with advanced solid malignancies (Rosen et al., 2007). Additional studies of motesanib as monotherapy and in combination with various agents are currently ongoing.

Definitive characterization of metabolites and examination of species differences in metabolism are becoming increasingly important.

This work was funded by Amgen Inc. (Thousand Oaks, CA).

[1] Current affiliation: Pharmacokinetics and Drug Metabolism, Pharmacology Department, Genomics Institute of the Novartis Research Foundation, San Diego, California.

[2] Drug Metabolism and Pharmacokinetics, Early Drug Development, Celgene Corporation, Summit, New Jersey.

Article, publication date, and citation information can be found at http://dmd.aspetjournals.org.

doi:10.1124/dmd.108.025742.

ABBREVIATIONS: VEGF, vascular endothelial growth factor; PDGF, platelet-derived growth factor; Kit, stem cell factor receptor; P450, cytochrome P450; UGT, UDP-glucuronosyltransferase; M3, oxidative metabolite of motesanib, pyridine *N*-oxide; M4, oxidative metabolite of motesanib, lactam (oxindole); M1, conjugative metabolite of motesanib, indoline *N*-glucuronide; HPLC, high-pressure liquid chromatography; DAD, diode array detector; GA, glucuronic acid; HLM, human liver microsome; M5, oxidative metabolite of motesanib, carbinolamine; Ma, conjugative metabolite of motesanib, indoline *N*-carbamoyl glucuronide; LC/MS/MS, liquid chromatography/tandem mass spectrometry; ESI, electrospray ionization; LC/MS, LC/mass spectrometry; Mx, oxidative *N*-dealkylated metabolite of motesanib, isonicotinic acid; Q-TOF, quadrupole time-of-flight; 1D, one dimensional; 2D, two dimensional; HMBC, heteronuclear multiple bond correlation; Mb, conjugative metabolite of motesanib, indoline *N*-glucose; Mc, conjugative metabolite of motesanib, indoline *N*-*N*-acetylglucosamine; M2, oxidative metabolite of motesanib, structure unassigned; Miv, oxidative *N*-dealkylated metabolite of motesanib, lactam of Mv; Mv, oxidative *N*-dealkylated metabolite of motesanib, 2-amino nicotinamide; CID, collision-induced dissociation; ILT-threo, L-threo isoleucine thiazolidide [(2*S*,3*S*)-3-methyl-1-oxo-1-(1,3-thiazolidin-3 yl)-pentan-2-amine fumarate (2:1)].

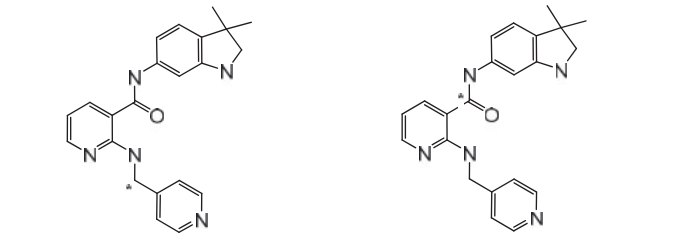

FIG. 1. Chemical structures of ^{14}C-labeled motesanib.

An understanding of quantitative and qualitative differences in metabolic profiles, especially with respect to metabolites unique to humans, is essential to comparing exposure and safety of a drug in nonclinical species relative to humans during risk assessment (Baillie et al., 2002; Hastings et al., 2003). In addition, identification of enzymes involved in the metabolism of a drug can help predict potential drug-drug interactions and variability in pharmacokinetics. In this study, we report results from the first preclinical metabolic investigation of motesanib. Phase I oxidative and phase II conjugative metabolites of motesanib were detected and characterized by using liver microsomes and hepatocytes from a mouse, rat, dog, monkey, and human. The cytochrome P450 (P450) isozymes responsible for oxidative metabolism of motesanib, as well as UDP-glucuronosyltransferase (UGT) isozymes involved in *N*-glucuronidation of motesanib, were also examined.

Materials and Methods

Chemicals and Reagents. Motesanib, authentic metabolite standards M3 (*N*-oxide), M4 (lactam), M1 (indoline *N*-glucuronide), and 2-[(1*H*-pyrrolo[2,3-b]-pyridin-4-ylmethyl)amino]-*N*-(1,2,3,4-tetrahydro-4,4-dimethyl-7-quinolinyl)-3-pyridinecarboxamide (internal standard used for P450 reaction phenotyping experiments) were synthesized at Amgen Inc. (Thousand Oaks, CA). [Methylene ^{14}C]motesanib (specific activity, 23 mCi/mmol) and [carbonyl ^{14}C]motesanib (specific activity, 54 mCi/mmol) (Fig. 1) were synthesized by Moravek Biochemicals, Inc. (Brea, CA). A 1-mM (25 or 50 μCi/ml) stock solution of [methylene ^{14}C]motesanib dissolved in acetonitrile was used.

Hydroxydiclofenac was purchased from BD Gentest (Woburn, MA). D9-OH-bufuralol was synthesized by PharmaCore (High Point, NC). All other reagents were purchased from Sigma-Aldrich (St. Louis, MO) and were of the highest quality available. The In-Flow 3 scintillant was purchased from IN/US Systems (Tampa, FL).

Hepatic microsomes from male CD-1 mice, male Sprague-Dawley rats, male beagle dogs, male cynomolgus monkeys, and humans (pooled gender mix) were purchased from Cedra (Austin, TX). Microsomes expressing human cDNA P450s (Supersomes), microsomes obtained from engineered cell lines expressing individual UGTs, and monoclonal antibodies specific for CYP3A4, CYP2D6, and CYP1A were obtained from BD Gentest.

Cryopreserved monkey and human hepatocytes were purchased from In Vitro Technologies (Baltimore, MD). Freshly isolated male beagle dog hepatocytes were purchased from XenoTech LLC, (Lenexa, KS). Hepatocytes were freshly isolated from 6- to 8-week-old male Sprague-Dawley rats (Charles River Laboratories, Inc., Wilmington, MA) and CD-1 mice (Charles River Laboratories Inc.). Rat and mouse hepatocytes were isolated by in situ liver perfusion with blanch and collagenase media. The perfused liver was removed, and cells were gently shaken into a calcium-free hepatocyte maintenance media. The nonhepatocyte cells, dead cells, and connective tissue remnants were removed from the viable hepatocytes by gently centrifuging and washing the cells three times with hepatocyte incubation media.

Oxidative Microsomal Incubations. [Methylene ^{14}C]motesanib (10 μM, 0.225 μCi/ml) was incubated with liver microsomes (1.0 mg/ml in 100 mM phosphate buffer, pH 7.4) from human, monkey, dog, mouse, and rat at 37°C for 30 min with or without 1 mM NADPH in a total volume of 0.5 ml. Incubations were stopped by adding 250 μl of ice-cold acetonitrile containing 0.1% formic acid followed by centrifugation at 14,000 rpm for 10 min. The supernatants were analyzed directly (without any further sample clean up) by high-performance liquid chromatography (HPLC) with a diode array detector (DAD) and a β-RAM radiometric detector. Selected samples were analyzed by HPLC with ion-trap mass spectrometry.

Phase II Microsomal Incubations. [Methylene ^{14}C]motesanib (10 μM, 0.225 μCi/ml) was incubated with liver microsomes (1.0 mg/ml in 100 mM phosphate buffer containing 10 mM magnesium chloride, pH 7.4) from human, monkey, dog, mouse, and rat, respectively, at 37°C for 30 min, with or without phase II cofactors UDP-glucuronic acid (GA), UDP-glucose, UDP-galactose, or UDP-*N*-acetylglucosamine (2 mM final concentration) in a total volume of 0.5 ml. Alamethicin (25 mg/ml in methanol) was added to the incubations at a final concentration of 100 μg/mg protein. Incubations were stopped by adding 250 μl of ice-cold acetonitrile followed by centrifugation at 14,000 rpm for 10 min. The supernatant was analyzed by HPLC with DAD and by radiometric detection. Selected samples were analyzed by HPLC with ion-trap mass spectrometry for metabolite identification. The percentages of these phase II conjugates quantified by their UV peak areas were identical to those quantified by radiometric detection. Subsequent measurements of *N*-glucuronide (M1) in UGT phenotyping and kinetic experiments were therefore based on UV peak areas, and no internal standard was used.

Hepatocyte Incubations. Hepatocytes were suspended in Krebs-Henseleit buffer at a cell concentration of 1×10^6 cells/ml. In a 24-well plate, [methylene ^{14}C]- or [carbonyl ^{14}C]motesanib was incubated at 10 μM (0.25 or 0.5 μCi/ml) in 0.5 ml of cell suspension with rat, mouse, monkey, dog, and human hepatocytes for 0, 2, and 4 h. The positive control was 7-ethoxy coumarin at a concentration of 50 μM. Incubations were conducted at 37°C in the presence of 5% CO_2 with saturating humidity and with gentle shaking every 10 to 15 min. Each treatment was performed in duplicate, and the incubations were terminated using 250 μl of acetonitrile. The total volume was transferred to a 1.5-ml conical centrifuge tube and vortexed and centrifuged, and the supernatant was frozen at −80°C until direct analysis by HPLC with radiometric detection and by mass spectrometry.

Metabolite Biosynthesis and Isolation for Nuclear Magnetic Resonance Spectroscopy Characterization. To isolate sufficient quantities (50–100 μg) of metabolites (M3, M4, and M5) for structural characterization by NMR spectroscopy, incubations of nonradioactive motesanib with mouse and human liver microsomes (HLMs) in the presence of NADPH were scaled up. Incubation conditions were first optimized for metabolite production in terms of motesanib concentration, microsomal protein concentration, and incubation time. Motesanib (50 μM) was then incubated with human or mouse liver microsomes (2 mg/ml) and 1 mM NADPH for 1 h in a total volume of 100 ml. To isolate enough M1 (~150 μg) for NMR confirmation, incubation of cold motesanib (25 μM) with human liver microsomes (1 mg/ml) in the presence of UDP-GA (2 mM) was also scaled up in a total volume of 20 ml and incubated for 1 h. Metabolite Ma was biosynthesized by incubating 0.25 mg/ml motesanib with 1 mg/ml monkey liver microsomes in potassium carbonate buffer (100 mM and saturated with dry ice). UDP-GA (2 mM), alamethicin (60 μg/mg microsomes), and D-saccharolactone (5 mM) were added, and the mixture was incubated in a closed-system CO_2 atmosphere at 37°C for 20 h.

Reactions were stopped by adding an equal volume of acetonitrile. Supernatants were diluted and extracted by solid-phase extraction [Oasis HLB (Waters, Milford, MA), 6 cc/500 mg, conditioned with 2×6 ml of methanol followed by 2×6 ml H_2O]. Metabolites were isolated by semipreparative HPLC using a YMC ODS-AQ (Waters) column (10 mm × 100 mm) at a flow rate of 5 ml/min. Separation was carried out using a linear gradient of 10% B to 90% B for 20 min (A = 90/10 H_2O/CH_3CN, 5 mM NH_4OAC; B = 90/10 CH_3CN/H_2O, 5 mM NH_4OAC). Isolated metabolites were concentrated and desalted using an Oasis HLB cartridge (1 cc/30 mg), eluted with methanol, and dried under nitrogen. The purities of metabolites were verified by HPLC and characterized by liquid chromatography/tandem mass spectrometry (LC/MS/MS). Samples were stored at −20°C before dissolving in methanol-d4 for NMR analysis.

Oxidative Metabolism of Motesanib by Recombinant Cytochrome P450 Isoforms. Incubations were performed with microsomes from engineered cell lines expressing individual P450s. Recombinant (Supersomes) CYP1A1+OR, 1A2+OR, 1B1+OR, 2A6+OR+b5, 2B6+OR+b5, 2C8+OR+b5, 2C9*1+OR+b5, 2C9*2+OR, 2C18+OR, 2C19+OR+b5, 2D6*1+OR, 2E1+OR+b5,

3A4+OR+b5, 3A5+OR, 3A7+OR+b5, and 4A11+OR were tested. Incubations were conducted with [methylene ^{14}C]motesanib (10 μM) and P450 isozyme (50 pmol/ml), with or without 1 mM NADPH, in a total volume of 300 μl at 37°C for 30 min. The incubations were quenched with 150 μl of ice-cold acetonitrile, vortexed, and centrifuged at 14,000 rpm for 10 min. Supernatants were analyzed by HPLC with UV and radiometric detection.

Inhibition of Motesanib Oxidative Metabolism by Selective Cytochrome P450 Inhibitors. For P450-mediated reactions, experimental conditions were optimized and linear conditions were established with respect to protein, time of incubation, and substrate concentration. Based on these results and the turnover of metabolites, a 10-μM motesanib concentration was selected to allow for formation of metabolites and to provide adequate signal and sensitivity for detection of significant inhibition (>90%) when incubated with inhibitors or antibodies. In addition, the concentrations used were projected to be within two times the maximal concentrations expected in the clinic at the time of the study. Inhibition studies with P450 isoform-selective chemical inhibitors were carried out using 10 μM motesanib with 1 mg/ml human liver microsomes in phosphate buffer (100 mM, pH 7.4) and 1 mM NADPH at 37°C for 30 min. Experiments were conducted using two different inhibitor concentrations in a total incubation volume of 200 μl (see *Results* for concentrations of each inhibitor). The reactions were stopped using 100 μl of ice-cold acetonitrile containing 0.6 μM internal standard (a proprietary structural analog of motesanib). The supernatants obtained after centrifuging for 10 min at 14,000 rpm were diluted using equal volumes of HPLC-grade water and analyzed by selected ion monitoring of metabolites using positive ion electrospray ionization (ESI) on an ion-trap mass spectrometer (LCQ classic; Thermo Fisher Scientific, Waltham, MA).

Control experiments were performed using known selective P450 substrates and inhibitors. The control probe reactions used included the following: phenacetin *O*-deethylation for CYP1A2, coumarin 7-hydroxylation for CYP2A6, diclofenac 4′ hydroxylation for CYP2C9, *S*-mephenytoin 4-hydroxylation for CYP2C19, bufuralol 1′ hydroxylation for CYP2D6, chlorzoxazone 6-hydroxylation for CYP2E1, and midazolam 1′-hydroxylation for CYP3A4. Mechanism-based inhibitors, such as 8-methoxypsoralen and diethyldithiocarbamate, were preincubated with microsomes and NADPH for 5 min before the addition of the respective substrates. Analysis of samples was performed using an API3000 triple quadrupole mass spectrometer (MDS Sciex, Concord, ON, Canada) by using specific multiple reaction monitoring transitions for the marker metabolites.

Inhibition of Motesanib Oxidative Metabolism by Specific Anti-P450 Antibodies. Human liver microsomes (2 mg/ml in phosphate buffer) were added to monoclonal antibodies (10 mg/ml) specific for CYP3A4, CYP2D6, and CYP1A at two different antibody concentrations (2 and 10 μg of IgG per 0.1 mg of microsomes) and incubated on ice for 15 min. Monoclonal antibodies specific for CYP1A were preincubated at room temperature for 30 min. Motesanib reaction mixtures (20 μM motesanib and 2 mM NADPH in 100 mM phosphate buffer, pH 7.4) were preincubated at 37°C for 5 min and added to equal volumes of each antibody mixture. Samples were incubated at 37°C for 30 min. Final concentrations of motesanib, NADPH, and monoclonal antibody were 10 μM, 1 mM, and 2 μg/0.1 mg microsomal protein or 10 μg/0.1 mg microsomal protein. Incubations were terminated by the addition of one half-volume of ice-cold acetonitrile containing 0.6 μM internal standard. Samples were vortexed and centrifuged for 10 min at 14,000 rpm and then analyzed by ion-trap mass spectrometry by using selected ion monitoring of metabolites, as in the case for selective chemical inhibitors.

Positive control experiments using probe substrates of CYP3A4 (midazolam), CYP2D6 (bufuralol), and CYP1A (phenacetin) were performed by using similar incubation conditions.

Motesanib *N*-Glucuronidation by Recombinant UGT Isoforms. Microsomes (Supersomes) from engineered cell lines expressing individual UGTs (UGT1A1, UGT1A3, UGT1A4, UGT1A6, UGT1A8, UGT1A9, UGT2B7, and UGT2B15) were tested for glucuronidation activity. UGT isozymes (0.5 mg/ml in 50 mM Tris-HCl buffer, 1 mM $MgCl_2$; pH 7.5) were preincubated with alamethicin (100 μg/mg microsomal protein) for 15 min on ice, and the motesanib substrate (10 μM) was added and preincubated at 37°C for 5 min. Reactions were initiated by adding 5 mM UDP-GA and incubated at 37°C for 30 min. Incubations were quenched with equal volumes of ice-cold acetonitrile, vortexed, and centrifuged. The supernatants were analyzed by HPLC with UV detection.

Inhibition of Motesanib *N*-Glucuronidation by Selective UGT Substrates/Inhibitors. The rate of formation of *N*-glucuronide metabolite M1 in human liver microsomes was linear for 10 min of incubation at a final protein concentration of 0.25 mg/ml in phosphate (100 mM), pH 7.4, containing 10 mM $MgCl_2$. Therefore, these reaction conditions were used for inhibition studies. The microsomal protein was preincubated with alamethicin on ice for 15 min (70 μg alamethicin/mg microsomal protein; alamethicin was prepared as a 25-mg/ml stock solution in methanol). Immediately before adding motesanib (final concentration, 10 μM), 1 or 5 mM imipramine or 25 or 50 μM bilirubin was added as a competitive inhibitor of UGT1A4 and UGT1A1. Reactions were initiated by adding 2 mM UDP-GA and then incubated at 37°C for 10 min. Incubations were quenched with 1 half-volume of ice-cold acetonitrile and then vortexed and centrifuged. The resulting supernatants were diluted using equal volumes of HPLC-grade water and then analyzed by HPLC with UV detection.

Enzyme Kinetics of Motesanib *N*-Glucuronidation in Humans, Rats, Dogs, and Monkeys. Incubation conditions for motesanib *N*-glucuronidation in human, rat, dog, and monkey liver microsomes were optimized for microsomal protein concentration and incubation time, and the incubations were conducted under initial-rate conditions. All incubations were conducted in phosphate buffer (100 mM) containing 10 mM $MgCl_2$ buffer (pH 7.4) and preincubated with 70 μg alamethicin/mg microsomal protein for 15 min before reaction initiation by 2 mM UDP-GA. To investigate the enzyme kinetics of *N*-glucuronidation in human liver microsomes, 1 to 400 μM motesanib was incubated with 0.25 mg/ml microsomal protein at 37°C for 10 min for motesanib concentrations up to 25 μM and for 30 min for motesanib concentrations higher than 25 μM. Using rat liver microsomes, 1 to 200 μM motesanib was incubated with 0.5 mg/ml microsomal protein at 37°C for 20 min. Using dog and monkey liver microsomes, 1 to 600 μM motesanib was incubated with 1 mg/ml microsomal protein at 37°C for 30 min. Incubations were stopped by adding 1 half-volume of ice-cold acetonitrile followed by centrifugation at 14,000 rpm for 10 min. The supernatants were diluted 1:1 with H_2O and analyzed by HPLC with a DAD (λ = 338 nm). Motesanib *N*-glucuronide (M1) quantification was based on the UV peak area. Kinetic data (K_m and V_{max}) were obtained using the Michaelis-Menten equation, curve fitting with simple weighting, and the least-squares minimization procedure (regression analysis) using SigmaPlot version 8.0 (Systat Software Inc., San Jose, CA).

Liquid Chromatography with Radiometric Detection and Liquid Chromatography/Mass Spectrometry Analysis. Samples from microsomal and hepatocyte metabolic-profiling experiments were analyzed by reverse-phase HPLC (Agilent 1100; Agilent Technologies, Santa Clara, CA) with diode array UV (λ = 338 nm) and a Flo-One (PerkinElmer Life and Analytical Sciences, Waltham, MA) or a β-RAM (IN/US Systems) radiochemical flow scintillation analyzer. Selected samples were also analyzed by HPLC with ion-trap mass spectrometry (LCQ classic; Thermo Fisher Scientific) by using ESI in positive-ion mode. Separation was performed using a Phenomenex Luna C18 column (3 μm, 4.6 × 150 mm; Phenomenex, Torrance, CA) and a mobile phase consisting of 90:10 (v/v) H_2O/CH_3CN containing 5 mM NH_4OAc (A) and 90:10 (v/v) CH_3CN/H_2O containing 5 mM NH_4OAc (B). Because some of the phase II metabolites were acid labile, acid was avoided in chromatographic analysis. A step gradient (0–2 min, 0% B, linear to 90% in 32 min, then to 100% at 32.1 min, held at 100% B until 40 min) at a flow of 1 ml/min was used. The LC flow after UV detection was split via a zero-volume tee with 80% of the flow to the β-RAM and 20% of the flow to the mass spectrometer. The β-RAM was equipped with a liquid flow cell of 500 μl, and the LC flow was mixed with liquid scintillant at a ratio of 1:3. Column recovery of injected sample radioactivity was evaluated by comparing the amount of radioactivity injected (determined using liquid scintillation counting) and the amount of total radioactivity detected by β-RAM. No loss of radioactivity on the column was found for either microsomal or hepatocyte samples.

Ion-trap mass spectrometer parameters were optimized by using a motesanib standard solution (1 μM). ESI source parameters were set at sheath gas, 80 (arbitrary units); auxiliary gas, 5; capillary, 275°C; collision energy, 35% (arbitrary units); and mass range, 100 to 750 amu.

In the P450-phenotyping experiments using chemical inhibitors and P450-specific antibodies, a shorter LC/mass spectrometry (LC/MS) method with a

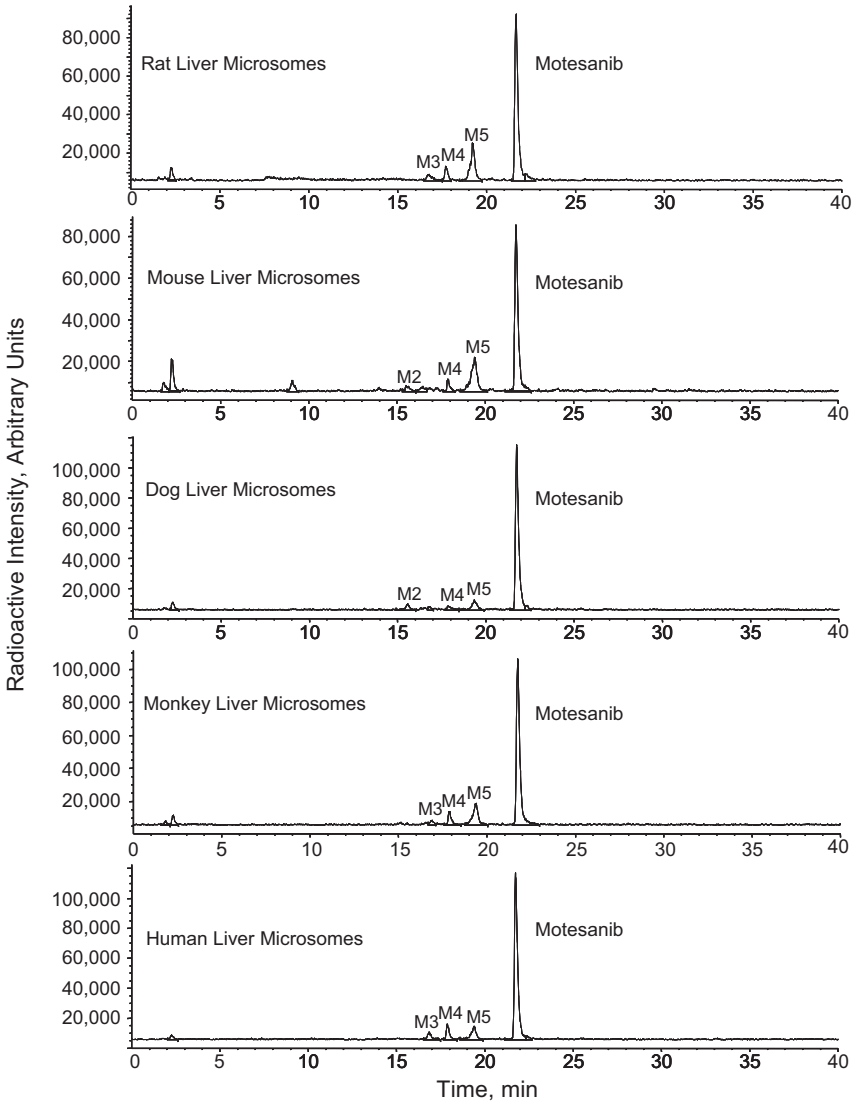

FIG. 2. In vitro oxidative metabolism profiles of motesanib in liver microsomes from human and preclinical species.

linear gradient of 15% B to 95% B (same mobile phase as stated above) in 10 min was used. The separation of motesanib and its metabolites was carried out using a YMC ODS-AQ column (3 μm, 2.0 $\times$ 50 mm) at a flow rate of 0.25 ml/min. Metabolites M3, M4, and M5 and the internal standard were detected by selected ion monitoring of 390.2, 388.2, 372.2, and 427.1 ions, respectively. The ratio of each metabolite's peak area to the internal standard was used to calculate the percentage of inhibition by chemical inhibitors or P450 antibodies.

Accurate Mass Spectrometry Analysis. High-resolution mass spectrometric measurements of Mx were performed by using a quadrupole time-of-flight (Q-TOF) mass spectrometer (API-US; Waters) equipped with a dual orthogonal Z SPRAY ESI source. Separation was performed by reverse-phase HPLC (Agilent 1100; Agilent Technologies), using acidic mobile phases (A = 0.1% formic acid in H_2O; B = 0.1% formic acid in acetonitrile) for better retention of Mx on the HPLC column. Concentrated samples from rat hepatocyte incubation of motesanib were injected into a YMC ODS-AQ C18 column (5 μm, 4.6 $\times$ 250 mm) at a flow rate of 1.0 ml/min with a 40-min gradient (0–5 min, 0% B; 5–35 min, linear to 60% B, 36 min, 95% B, held until 40 min). Q-TOF was operated under V-Mode and calibrated with polyethyleneglycol; 1 μg/ml reserpine was used as lock spray at a flow rate of 3 μl/min.

NMR Spectroscopy Analysis. The structures of motesanib metabolites M1, Ma, M3, M4, and M5 were solved by NMR analysis and by acquiring a combination of one-dimensional (1D) proton, two-dimensional (2D) ^{1}H-^{1}H homonuclear correlation spectroscopy, 2D ^{1}H-^{1}H nuclear Overhauser effect spectroscopy, 2D ^{1}H-^{13}C heteronuclear single-bond correlation, and 2D ^{1}H-^{13}C heteronuclear multiple-bond correlation (HMBC) spectra using 600 MHz NMR spectrometers (Bruker BioSpin Inc., Billerica, MA) equipped with either a 5-mm broadband inverse probe (Nalorac/Varian Inc., Palo Alto, CA) or 5-mm TCI CryoProbe (Bruker BioSpin Inc.). Purified metabolites (M1, M3, M4, and M5; 20–120 μg) were dissolved in 300 μl of methanol-d4 and transferred to 5-mm susceptibility-matched Shigemi tubes (Shigemi Inc., Allison Park, PA). Isolated metabolite Ma was dissolved in 160 μl of MeOD-d4 and transferred to a 3-mm tube. All spectra were recorded with standard experiments by using a Bruker pulse program library. Spectral resolution for 1H was 0.3 Hz/pt and 3 Hz/pt in 1D and 2D experiments, respectively.

Results

Liver Microsomal Oxidative Metabolism of Motesanib. Several oxidative metabolites were observed in incubations of both human and animal liver microsomes. The microsomal oxidative profiles of motesanib and the percentages of motesanib and its oxidative metabolites relative to the total radioactivity are shown in Fig. 2 and Table 1. Among the species investigated, mouse liver microsomes exhibited the highest extent of in vitro oxidative metabolism of motesanib. All metabolites formed in human liver microsomes were also detected in other species.

Hepatocyte Metabolism of Motesanib. Motesanib was extensively metabolized in hepatocyte incubations, especially in human hepatocytes, which had approximately 15% motesanib remaining after

TABLE 1

The composition of oxidative metabolites of motesanib in microsomes across species

Species	Distribution of Metabolites in Microsomal Incubations[a]						
	Mx	M2	M3	M4	M5	Parent	Others[b]
Rat	8.2	ND	4.2	5.9	17.5	62.4	ND
Mouse	12.3	3.6	1.0	3.8	18.3	52.7	7.2
Dog	4.7	4.0	3.8	3.0	8.1	74.9	1.5
Monkey	5.5	ND	3.3	5.7	14.6	67.8	2.2
Human	2.8	ND	5.3	6.6	10.2	75.1	ND

ND, not detected.

[a] Results obtained by HPLC with a β-RAM radiometric detector. Numbers indicate mean percentages, which represent the compositions of microsomal incubations ($n = 2$ for each species) using 10 μM motesanib and 1 mg/ml microsomal protein incubated in the presence of 1 mM NADPH at 37°C for 30 min.

[b] Peaks not identified by LC/MS.

4 h of incubation (Fig. 3; Table 2). Phase II conjugative pathways (M1, Ma, Mb, and Mc) accounted for 53, 47, 31, 81, and 93% of total metabolism in rat, mouse, dog, monkey, and human hepatocytes, respectively. The major human metabolite was M1 (indoline *N*-glucuronide), which accounted for >90% of total metabolism and was also formed in all other species examined. The phase II conjugates Ma (*N*-carbamoyl glucuronide) and Mb (*N*-glucose) were detected in rat, monkey, mouse, and dog hepatocyte incubations, but not in human hepatocytes. Metabolite Mc (*N*-acetylglucosamine conjugate) was detected only in monkey hepatocyte incubations. In addition to the phase II conjugates, oxidative metabolites such as M2, M3, M4, and M5 were also detected in some species (Fig. 3; Table 2). Metabolites resulting from *N*-dealkylation of methyl pyridyl, Mx, Miv and Mv, were also detected.

Liver Microsomal Phase II Metabolism of Motesanib. The species differences observed in the formation of the phase II conjugates

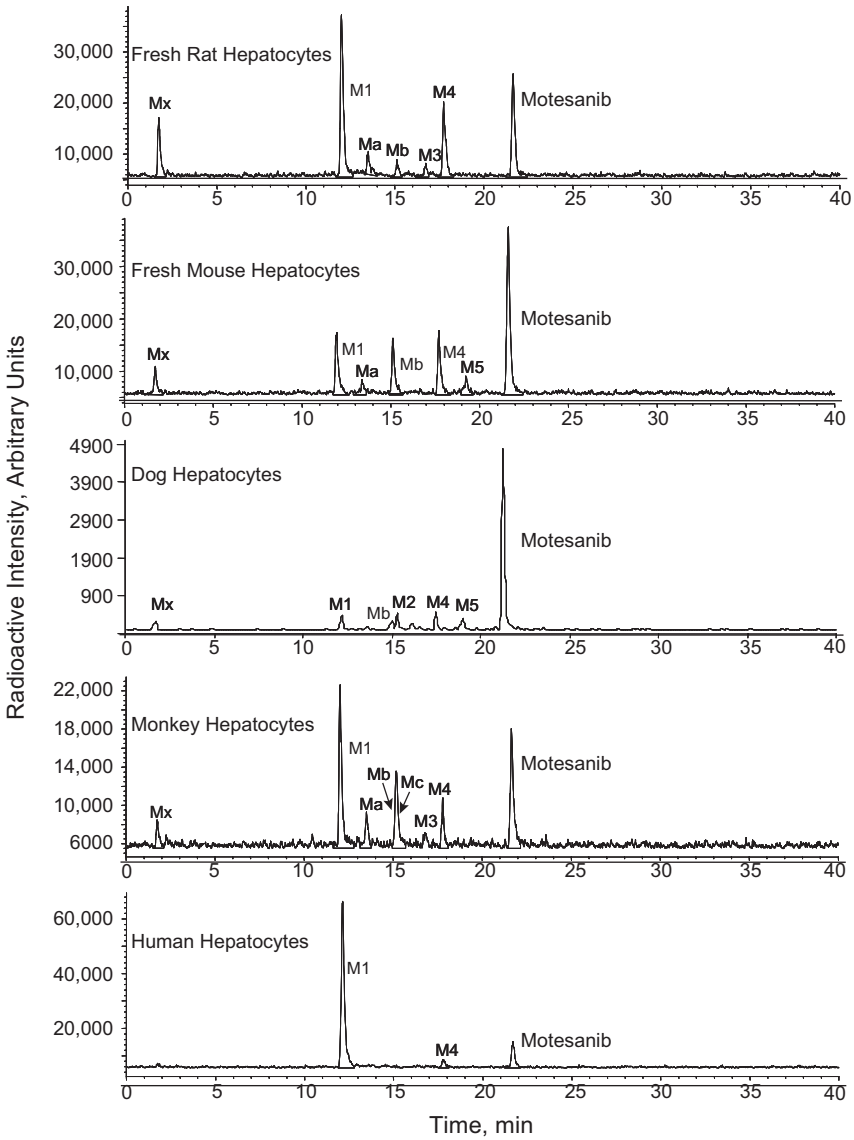

FIG. 3. In vitro metabolism profiles of motesanib in hepatocytes from human and preclinical species.

TABLE 2

The composition of oxidative and conjugative metabolites of motesanib in hepatocytes across species

Species	Distribution of Metabolites in Hepatocyte Incubations[a]										
	Mx	M1	Ma	Mb	Mc	M2	M3	M4	M5	Parent	Others
Rat	11.0	29.2	6.2	3.3	ND	ND	3.2	20.2	ND	27.0	ND
Mouse	5.3	11.7	3.0	10.8	ND	ND	ND	16.6	6.8	45.9	ND
Dog	3.4	7.2	ND	3.8	ND	4.5	ND	5.6	6.4	64.9	4.2
Monkey	4.9	33.0	7.1	7.2	11.1	ND	ND	8.9	ND	27.9	ND
Human	ND	79.3	Trace	ND	ND	ND	1.4	4.7	ND	14.7	ND

ND, not detected.

[a] Results obtained by HPLC with a β-RAM radiometric detector. Numbers indicate mean percentages, which represent the compositions of hepatocyte incubations (n = 2 or 3) using 10 μM motesanib and hepatocytes (1×10^6 cells/ml) at 37°C for 4 h.

M1, Mb, and Mc were further examined in liver microsomes by using different UDP-sugar cofactors. The *N*-glucuronide metabolite M1 was formed in all species examined (Fig. 4; Table 3). The rate and extent of M1 formation was much greater in human liver microsomes than in other species. The *N*-glucose adduct Mb was formed in the presence of UDP-glucose in all species except human, and the highest rate of its formation was in monkey liver microsomes (Table 3). No adduct was detected in any of the species examined using UDP-galactose as a cofactor. When motesanib was incubated with liver microsomes using UDP-*N*-acetylglucosamine as a cofactor, only monkey liver microsomes generated the *N*-acetylglucosamine conjugate Mc (Table 3). Overall, the results obtained using liver microsomes agreed with results obtained using hepatocyte incubations.

Identification of Metabolites. Preliminary identification of metabolites was based on LC/MS, LC/MS/MS, and NMR. Using full-scan positive-ion ESI, motesanib and most of its metabolites were found to occur predominantly as protonated molecules $[M+H]^+$. Therefore, the molecular weight of each metabolite was readily obtained. Furthermore, multistage mass spectra obtained from ion-trap mass spectrometry of motesanib and its metabolites were generated using positive- or negative-ion ESI to identify the potential sites of metabolism. A summary of molecular ions and fragment ions of motesanib and its metabolites is shown in Table 4.

Motesanib. The molecular ion of motesanib $[M+H]^+$ was observed at *m/z* 374, and the peak at 2 mass units higher (*m/z* 376) corresponds with [^{14}C]motesanib (Fig. 5). The fragmentation of the $[M+H]^+$ ion

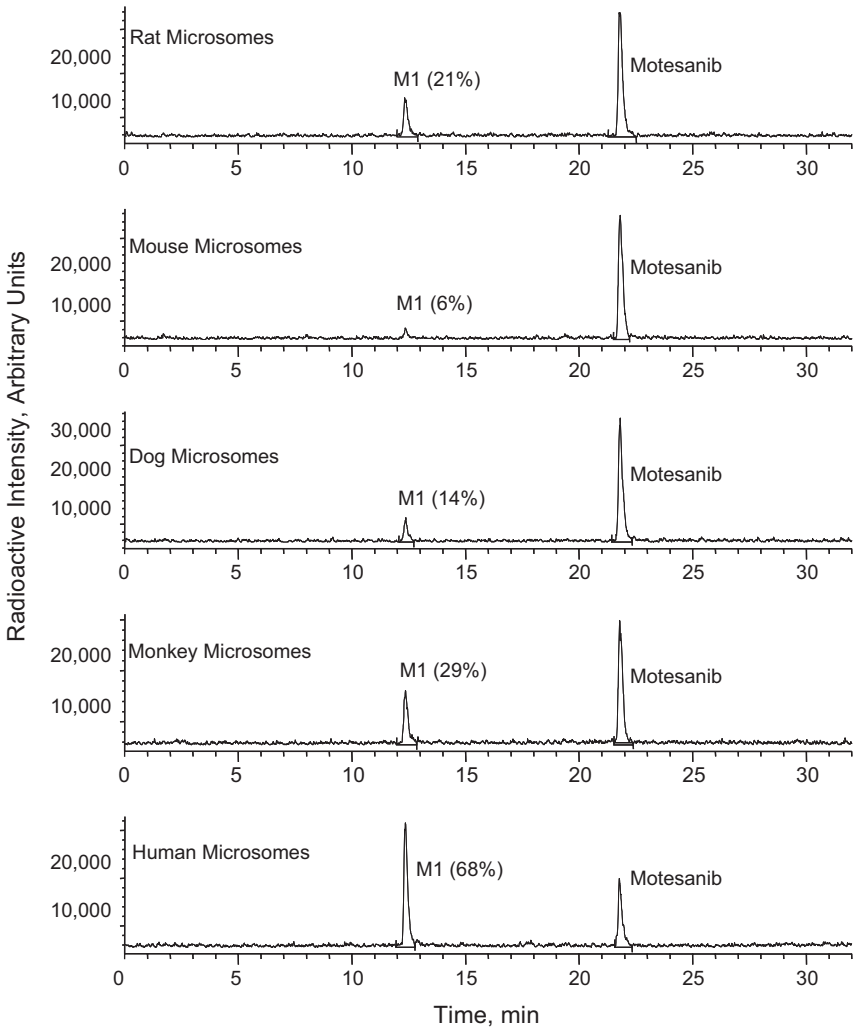

FIG. 4. Formation of motesanib *N*-glucuronide (M1) in liver microsomes across species with UDP-GA cofactor.

TABLE 3

The composition of conjugative metabolites of motesanib in microsomes across species

Cofactor	Metabolite	Percentage of Metabolite Formation[a]				
		Rat	Mouse	Dog	Monkey	Human
UDP-GA	M1	20.5	6.6	13.6	28.5	67.7
UDP-glucose	Mb	5.1	9.3	3.1	46.2	ND
UDP-*N*-acetylglucosamine	Mc	ND	ND	ND	24.4	ND

ND, not detected.

[a] Results obtained by HPLC with a β-RAM radiometric detector. Percentages represent mean relative amount of conjugative metabolites M1, Mb, and Mc formed in microsomal incubations (n = 2 for each species) using 10 μM motesanib and 1 mg/ml microsomal protein incubated in the presence of cofactor (2 mM) at 37°C for 30 min.

TABLE 4

CID mass spectra of motesanib and its in vitro metabolites

Metabolite	$[M+H]^+$, *m/z*	Major LC/MS/MS Fragments, *m/z*	Identity
Parent drug	374	212, 189	Motesanib
Mx	124		Isonicotinic acid
M2	388	370, 212, 159	
M3	390	372, 282, 252	*N*-oxide
M4	388	212	Lactam (oxindole)
M5	372	212, 187	Carbinolamine
M1	550	532, 374, 212, 189	Indoline *N*-glucuronide
Ma	594	418, 374	Indoline *N*-carbamoyl glucuronide
Mb	536	518, 374	Indoline *N*-glucose
Mc	577	374, 212, 189	Indoline *N*-*N*-acetylglucosamine
Mv	283	189, 121	2-Amino nicotinamide metabolite
Miv	297	121	Lactam of Mv

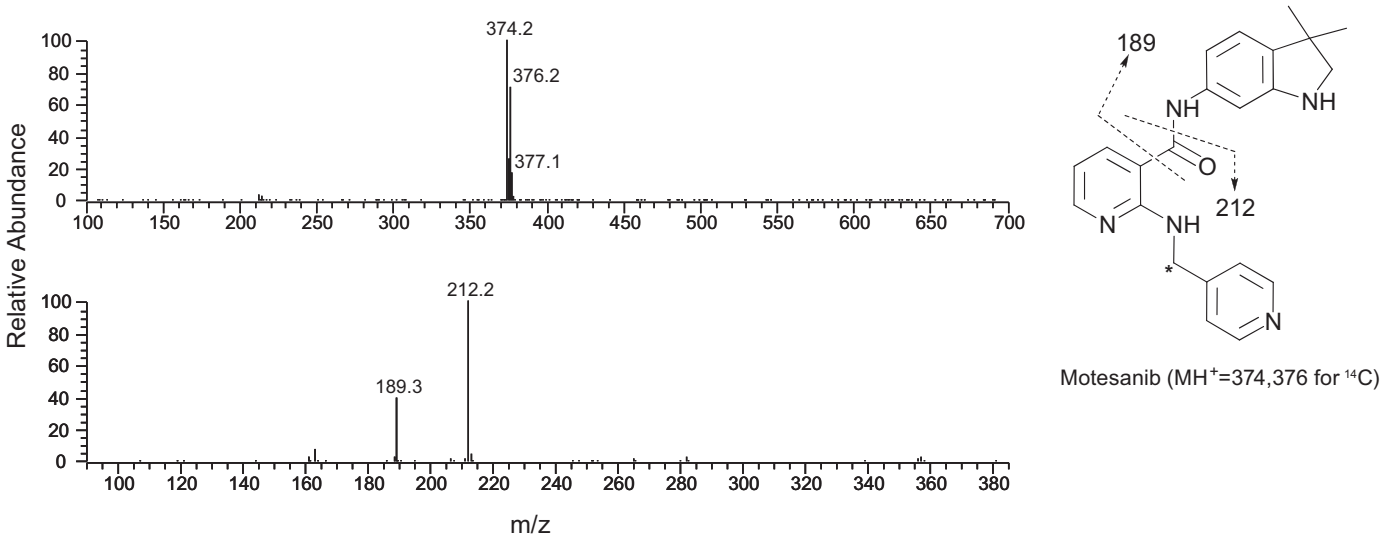

FIG. 5. Positive-ion ESI full-scan and tandem mass spectra of motesanib.

at *m/z* 374 generated by collision-induced dissociation (CID) was interpreted and used to aid in the structural assignment of the metabolites. The tandem mass spectrum of the $[M+H]^+$ ion at 35% collision energy (arbitrary unit) displayed 2 major fragment ions at *m/z* 212 and 189. Fragment ion at *m/z* 212 corresponded to the cleavage of nicotinamide amide bond and charge retention on 1 pyridyl moiety. Fragment ion at *m/z* 189 corresponded to the indoline formamide moiety. The proton NMR chemical shifts and coupling constants of motesanib are included in Table 5.

Metabolite M3. M3 exhibited molecular ion $[M+H]^+$ at *m/z* 390 in the ESI positive-ion full-scan mass spectrum, implying a monooxygenated metabolite (Fig. 6). The tandem mass spectrum of protonated M3 showed a major fragment ion at *m/z* 372, corresponding to the loss of H_2O, and two other minor fragment ions at *m/z* 282 and 252, probably resulting from cleavage of the methyl pyridyl group. The results of the negative-ion tandem mass spectra of M3 were in agreement with the positive-ion tandem mass spectra, suggesting that oxidation probably occurred on the methyl pyridyl moiety. This oxidation induced a fragmentation in M3 that is quite different from that of motesanib. The structural identity of M3 was confirmed to be pyridyl *N*-oxide by NMR analysis of the isolated M3 from microsomal incubations. The position of the *N*-oxide moiety was determined by the characteristic changes in chemical shifts and coupling pattern of protons H1 and H2, relative to motesanib, as shown in Table 5. The structure was further confirmed by comparison with a synthetic *N*-oxide standard, which showed chromatographic, mass spectral, and NMR characteristics identical to isolated metabolite M3.

Metabolite M4. Motesanib metabolite M4 was generated in vitro in both microsomal incubations and hepatocyte incubations of all species investigated. ESI positive-ion full-scan MS of M4 showed predomi-

TABLE 5

NMR characteristics of motesanib and its metabolites M3, M4, M5, M1, and Ma

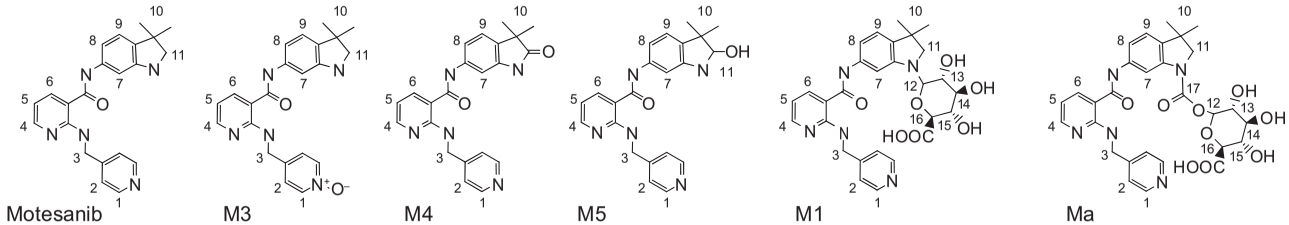

	Metabolite[a]									
	Motesanib		M3		M4	M5	M1		Ma	
Position	^{1}H (ppm) (mult, J in Hz)	^{13}C (ppm)	^{1}H (ppm) (mult, J in Hz)	^{13}C (ppm)	^{1}H (ppm) (mult, J in Hz)	^{1}H (ppm) (mult, J in Hz)	^{1}H (ppm) (mult, J in Hz)	^{13}C (ppm)	^{1}H (ppm) (mult, J in Hz)	^{13}C (ppm)
1	8.45 (d, 6)	146.5	8.28 (d, 6.7)[b]	138.0	8.46 (d, 6)	8.46 (m)	8.45 (d, 6)	148.1	8.44 (br)	148.0
2	7.43 (d, 6)	123.0	7.56 (d, 6.7)[b]	124.8	7.44 (d, 6)	7.45 (m)	7.43 (d, 6)	122.1	7.44 (d, 6.1)	122.3
3	4.78 (s)	43.1	4.78 (s)	42.2	4.8 (s)	4.82 (s)	4.79 (s)	42.7	4.78 (s)	42.8
4	8.12 (dd, 4.7, 1.7)	150.4	8.14 (dd, 4.7, 1.7)	150.3	8.16 (dd, 4.7, 1.7)	8.16 (dd, 4.7, 1.7)	8.11 (dd, 4.7, 1.7)	150.4	8.11 (d, 4.2)	150.5
5	6.7 (dd, 7.7, 4.7)	111.5	6.72 (dd, 7.7, 4.7)	111.4	6.73 (dd, 7.7, 4.7)	6.74 (dd, 7.7, 4.7)	6.7 (dd, 7.7, 4.7)	111.3	6.69 (dd, 7.8, 5.1)	111.4
6	8.04 (dd, 7.7, 1.7)	136.7	8.04 (dd, 7.7, 1.7)	136.5	8.08 (dd, 7.7, 1.7)	8.12 (dd, 7.7, 1.7)	8.06 (dd, 7.7, 1.7)	136.7	8.07 (dd, 7.8,1.6)	136.4
7	7.08 (d, 1.7)	104.8	7.08 (d, 1.7)	103.5	7.51 (m)[c]	7.04 (d, 1.7)	6.89 (d, 1.7)	101.4	7.42 (br)	116.4
8	6.94 (dd, 8.1, 1.7)	113.4	6.94 (dd, 8.1, 1.7)	112.0	7.25 (m)[c]	6.9 (dd, 8.1, 1.7)	7.06 (dd, 8.1, 1.7)	111.6	8.07 (br)	108.2
9	7.02 (d, 8.1)	121.6	7.03 (d, 8.1)	121.3	7.25 (m)[c]	7 (d, 8.1)	6.99 (d, 8.1)	121.3	7.19 (d, 8.2)	121.8
10	1.31 (s)	26.4	1.32 (s)	26.4	1.38 (s)	{1.32, 1.24}[d]	1.38 (s)	25.5	1.36	27.2
10′							1.29 (s)	27.8		
11	3.29 (s)	60.8	3.3 (s)	61.2	NA	4.52 (s)	3.44, 3.59[e]	59.9	3.82, 3.92[e]	62.0
12							4.82 (d, 8.9)	85.3	5.57 (d, 7.1)	95.2
13							3.6 (t, 8.5)	70.6	3.52 (br)	71.8
14							3.53 (t, 8.5)	77.9	3.52 (br)	76.3
15							3.49 (t, 8.5)	72.3	3.48 (br)	72.1
16							3.73 (t, 8.5)	77.0	3.82 (br)	75.3
17										151.3

Notations: Br, broad peak; d, doublet; dd, doublet of a doublet; Hz, Hertz; J, scalar coupling; m, multiplet; mult, multiplicity; NA, not available; ppm, parts per million; s, singlet.

[a] All spectra were acquired in MeOD-d_4 and internally referenced to solvent (CD2HOD) resonance at δ_H 3.32/δ_C 47.8 ppm. All signal integrals in 1D 1H NMR spectra were consistent with the spectral assignments.

[b] Pseudo doublet, strongly coupled AA′BB′.

[c] Strongly coupled ABX spin system.

[d] The 2 methyls are diastereotopic.

[e] AB multiplet.

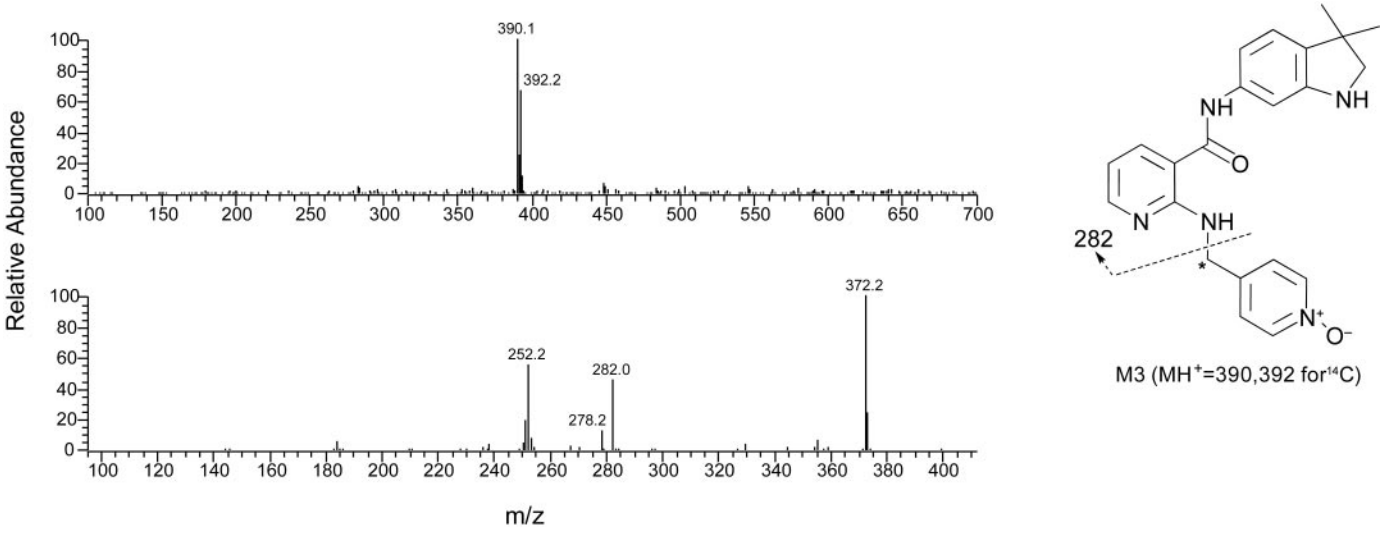

FIG. 6. Positive-ion ESI full-scan and tandem mass spectra of motesanib metabolite M3.

nantly a protonated molecule at *m/z* 388, 14 amu higher than that of protonated motesanib. The MS/MS of protonated M4 produced 1 major fragment ion at *m/z* 212 (Fig. 7), so the 14-amu increment must have occurred on the indoline moiety. The structure of M4 was confirmed by NMR analysis of the isolated M4 from microsomal incubations, and its proton NMR characteristic is shown in Table 5. The key observation in this experiment was the long-range methyl protons to carbonyl carbon (at 185 ppm) coupling from an HMBC experiment. The structure of M4 was also confirmed with cochromatography with authentic standards.

Metabolite M5. M5 was one of the major microsomal metabolites of motesanib detected in all species investigated (Fig. 2; Table 1). The positive-ion full-scan ESI spectrum of M5 clearly showed a predominant ion at *m/z* 372 (Fig. 8), 2 amu less than that of protonated motesanib (Fig. 5). As shown in Fig. 8, the tandem mass spectrum of M5 was similar to that of protonated motesanib, except that the fragment at *m/z* 189 for motesanib was shifted 2 amu less to *m/z* 187. NMR analysis of M5 (Table 5) indicated that it was a carbinolamine. The carbinolamine metabolite dehydrated readily during the ESI process, generating dehydrated ions in both positive- and negative-ion modes. The key observations in the HMBC experiment were long-range proton-carbon couplings 10(10′)-C11(C11′), where δ_{C11} = 100.3 ppm, $^{1}J_{C11\text{-}H11}$ = 161 Hz, $\delta_{C11'}$ = 182.4 ppm, and $^{1}J_{CH}$ = 182 Hz. The NMR data were essential to determining the structure of M5.

Metabolite M2. Metabolite M2 was a minor metabolite detected in mouse and dog microsomal incubations with motesanib (Fig. 2; Table 1). The ESI positive-ion full-scan mass spectrum of M2 exhibited predominantly an ion at *m/z* 388, a 14-amu increment comparable with that of protonated motesanib (data not shown). The M2 tandem mass spectrum was different from that of M4, and showed several diagnostic fragment ions at *m/z* 370, 212, and 159, suggesting that oxidation occurred on the indoline moiety. Therefore, M2 is possibly a sequential metabolite from M5. However, complete structure assignment of M2 was not possible based on MS data alone.

Metabolite M1. Motesanib metabolite M1 was the major metabolite formed in human hepatocytes (Fig. 3; Table 2). M1 was also formed in hepatocyte incubations of other species examined, but to a lesser extent than in the human sample. When motesanib was incubated with liver microsomes in the presence of UDP-GA, M1 was detected in all species. However, human liver microsomes exhibited the highest percentage of M1 formation (Fig. 4; Table 3).

The ESI positive-ion full-scan mass spectrum of M1 showed predominantly the $[M+H]^+$ ion at *m/z* 550, which is 176 amu higher than that of protonated motesanib and suggests direct glucuronidation of motesanib. The tandem mass spectrum of M1 displayed an abundant fragment ion at *m/z* 374 corresponding to the loss of a glucuronide moiety from motesanib (Fig. 9).

M1 was isolated from in vitro experiments and fully characterized by NMR. Identifiable proton and carbon chemical shifts are listed in Table 5. The 1D proton spectrum displayed chemical shifts from both motesanib and glucuronide moieties. The glucuronide anomeric proton appeared as a doublet at δ_H 4.82/δ_C 85.3 ppm, and its large H12–H13 scalar coupling (8.9 Hz) indicates a β-configuration at the anomeric carbon. HMBC correlations were observed between the methylene carbon in the indoline ring (C11, 59.9 ppm) and the anomeric proton (H12) of the glucuronide, and a 1D slice from the 2D ^{13}C-^{1}H HMBC spectrum at the chemical shift of C11 is displayed in Fig. 10. The 3-bond correlations to the anomeric proton and both methyl protons confirm that glucuronic acid is attached to the indoline nitrogen. In addition, the indoline *N*-glucuronide authentic standard was synthesized and showed identical chromatographic, mass spectral, and NMR characteristics compared with the isolated M1.

Metabolite Ma. Motesanib metabolite Ma was detected in hepatocyte incubations of several species (Fig. 3; Table 2). The ESI positive-ion full-scan mass spectrum of Ma identified predominantly the $[M+H]^+$ ion at *m/z* 594. The protonated Ma fragmented exclusively to *m/z* 418 upon CID, and the neutral loss of 176 amu again indicated glucuronide conjugation. MS^3 further revealed a neutral loss of 44 amu (CO_2) to produce protonated motesanib at *m/z* 374 as the predominant ion. Therefore, the structure of Ma was proposed to be *N*-carbamoyl glucuronide.

Ma was also formed in the in vitro incubations of motesanib with liver microsomes from several species in a CO_2-rich atmosphere in carbonate buffer and in the presence of UDP-GA. The reaction in monkey liver microsomes was scaled up, and under the experimental conditions, 30% of Ma and 10% of M1 were formed. Ma was isolated, purified, and fully characterized by NMR spectra. Its identifiable chemical shifts are listed in Table 5. The 1D proton spectrum of the metabolite showed peaks from both motesanib and glucuronide. Comparison of chemical shifts from motesanib and Ma indicated that changes were localized to the indoline moiety. The anomeric proton appeared at 5.57 (d, 7.1 Hz, β-anomer) with a carbon chemical shift

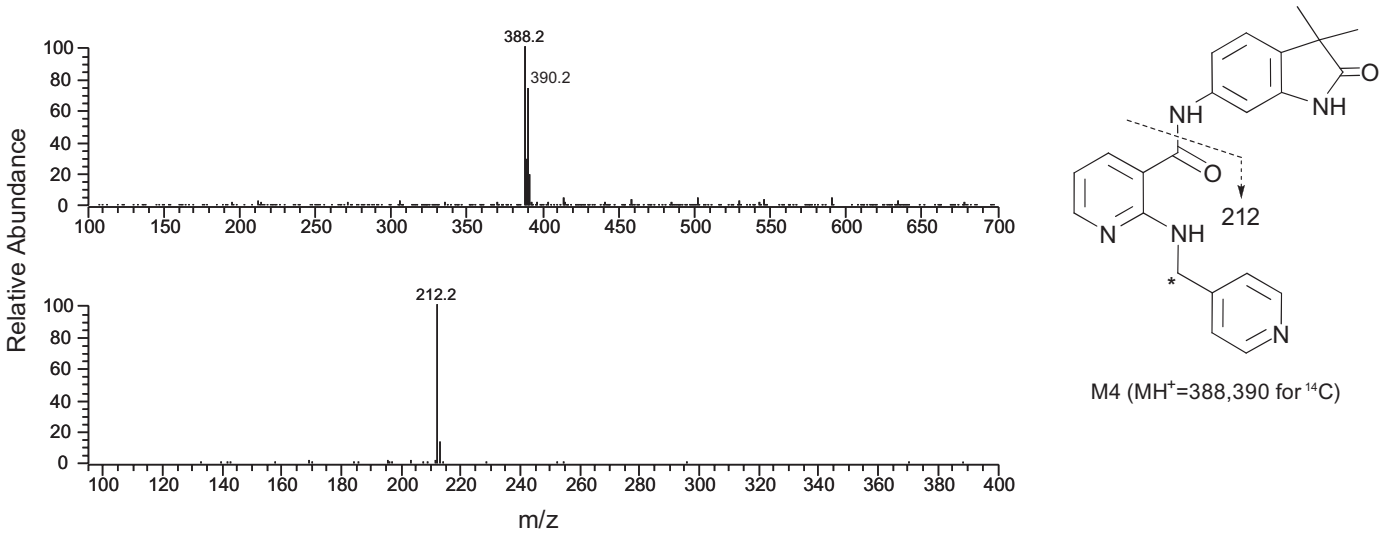

FIG. 7. Positive-ion ESI full-scan and tandem mass spectra of motesanib metabolite M4.

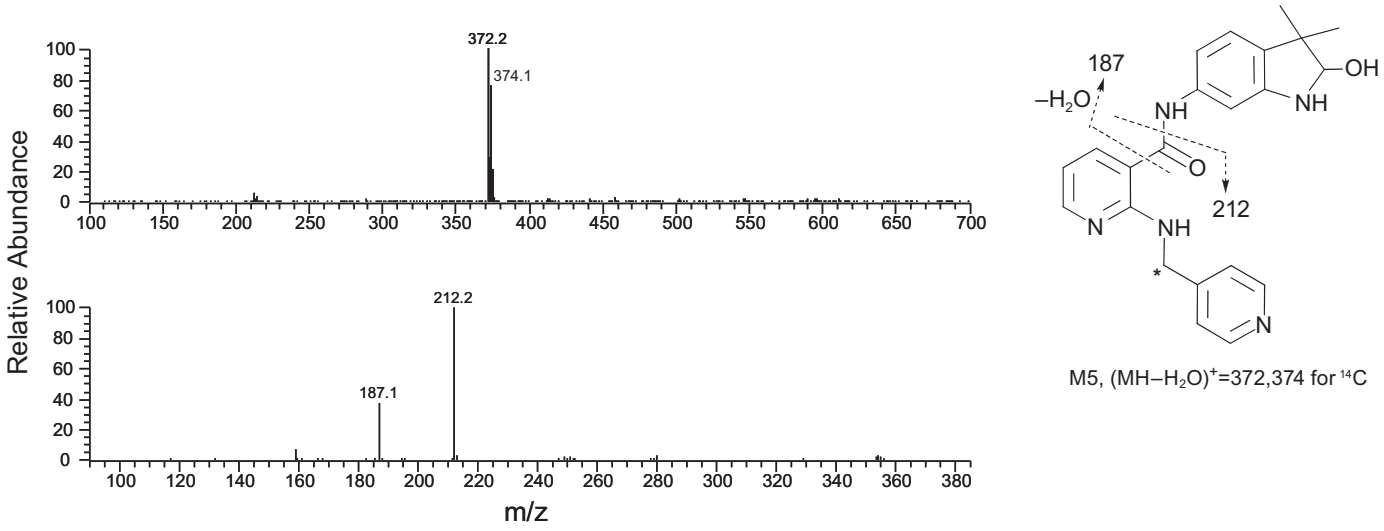

FIG. 8. Positive-ion ESI full-scan and tandem mass spectra of motesanib metabolite M5.

of 95.2 ppm, indicating an *O*-glucuronide. HMBC correlations were also observed from H11 to the carbonyl carbon (C17) at 151.5 ppm. The combined evidence strongly supports the presence of an *N*-carbamoyl glucuronide and the site of conjugation being on the indoline nitrogen.

Metabolite Mb. Motesanib metabolite Mb was detected in hepatocyte incubations of several species other than humans (Fig. 3; Table 2). Mb exhibited molecular ion $[M+H]^+$ at *m/z* 536. MS/MS of protonated Mb produced abundant fragment ions at *m/z* 374 and 518, which correspond to the intact protonated motesanib and loss of H_2O from Mb, respectively. Incubation of motesanib with liver microsomes of several species in the presence of UDP-glucose also yielded Mb (Table 3), but similar incubations in the presence of UDP-galactose did not. The structure of Mb was therefore identified as an *N*-glucose conjugate of motesanib, and the site of conjugation was probably on the indoline nitrogen, which is the site of conjugation for glucuronidation (M1 and Ma). Mb was not detectable in human liver microsomal incubations, which was consistent with the results from human hepatocyte incubation.

Metabolite Mc. Motesanib metabolite Mc was detected in monkey hepatocyte incubations, but not in other species (Fig. 3; Table 2). Mc exhibited molecular ion $[M+H]^+$ at *m/z* 577 in the positive-ion ESI mass spectrum. MS/MS of protonated Mc produced predominantly a fragment ion at *m/z* 374 corresponding to the intact protonated motesanib. Further fragmentation of the 374 ion produced ions at *m/z* 212 and 189 in the MS^3 spectrum. Mass spectrometry data indicated direct conjugation and a mass increment of 203 amu, and the conjugate moiety contained an odd number of nitrogen atoms. As a result, Mc was proposed to be an indoline *N*-linked *β*-*N*-acetylglucosamine adduct of motesanib. Because in vitro experiments using motesanib incubated with monkey liver microsomes in the presence of UDP-*N*-acetylglucosamine also produced the same metabolite (Table 3), the structure of Mc was confirmed to be the *β*-*N*-acetylglucosamine adduct of motesanib, and the site of conjugation is probably on the indoline nitrogen based on unequivocally assigned M1 and Ma metabolites. Both microsomal incubations in the presence of UDP-*N*-acetylglucosamine and hepatocyte incubations indicated that Mc was a unique metabolite formed in monkeys.

Metabolites Miv and Mv. Motesanib metabolites Miv and Mv were not detected by radiometry when [methylene ^{14}C]motesanib was used as substrate, but they were detected by UV and MS. Miv and Mv did not retain the radiolabel after *N*-dealkylation of the methyl pyridyl

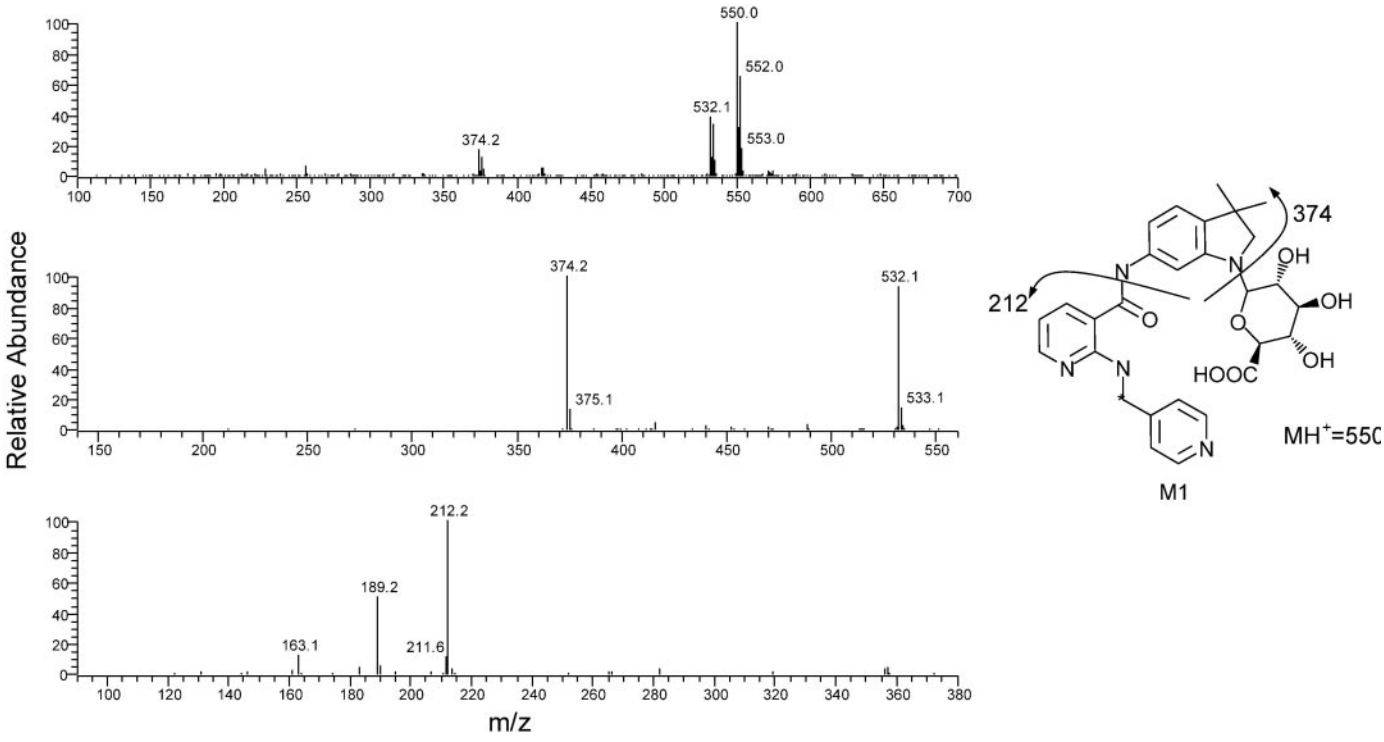

FIG. 9. Positive-ion ESI full-scan and tandem mass spectra of motesanib metabolite M1.

moiety. When [carbonyl ^{14}C]motesanib was incubated with rat hepatocytes, Miv and Mv, but not Mx, were detected by radiometry (Fig. 11), which confirmed that Miv and Mv were metabolites resulting from the loss of methyl pyridine and that Mx contained the methyl pyridyl moiety.

The ESI full-scan mass spectrum of Mv showed an abundant ion at *m/z* 283, and its tandem mass spectrum exhibited 2 unique fragment ions at *m/z* 189 and 121. Consequently, the identity of Mv has been proposed to be an amino nicotinamide metabolite. Metabolite Miv eluted earlier than Mv, and it exhibited a molecular ion at *m/z* 297, 14 amu higher than that of Miv. The tandem mass spectrum of protonated Miv revealed a predominant ion at *m/z* 121, suggesting that the amino pyridine moiety remained unchanged. Thus, the structure of Miv was proposed to be the lactam of Mv.

Metabolite Mx. Motesanib metabolite Mx was an extremely polar metabolite that eluted in the solvent front under analysis conditions. In comparison, Mx was better retained on a YMC ODS-AQ column using acid mobile phases. Using positive-ion ESI on the Q-TOF mass

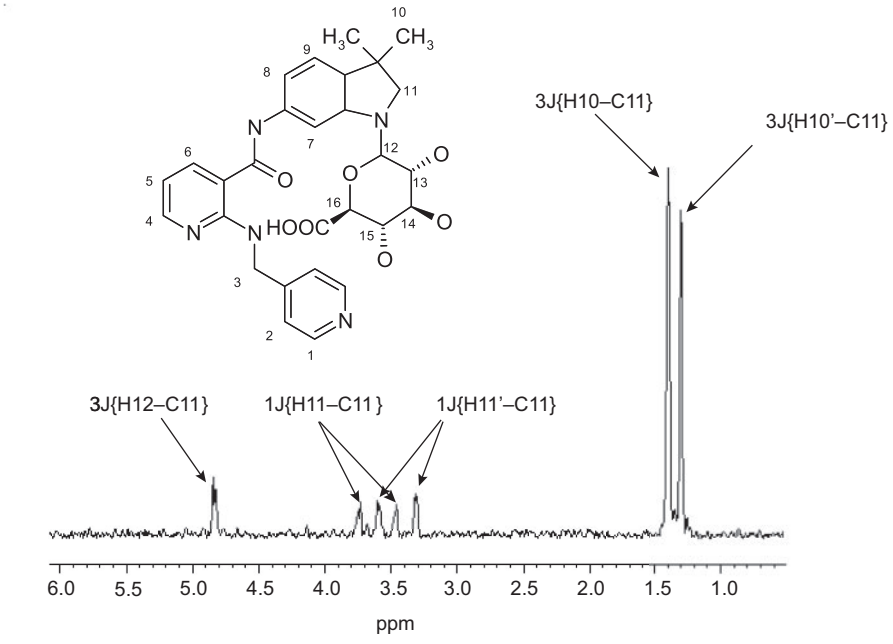

FIG. 10. One-dimensional proton trace extracted from 2D ^{13}C-^{1}H correlation spectrum of metabolite M1 at carbon chemical shift of C11.

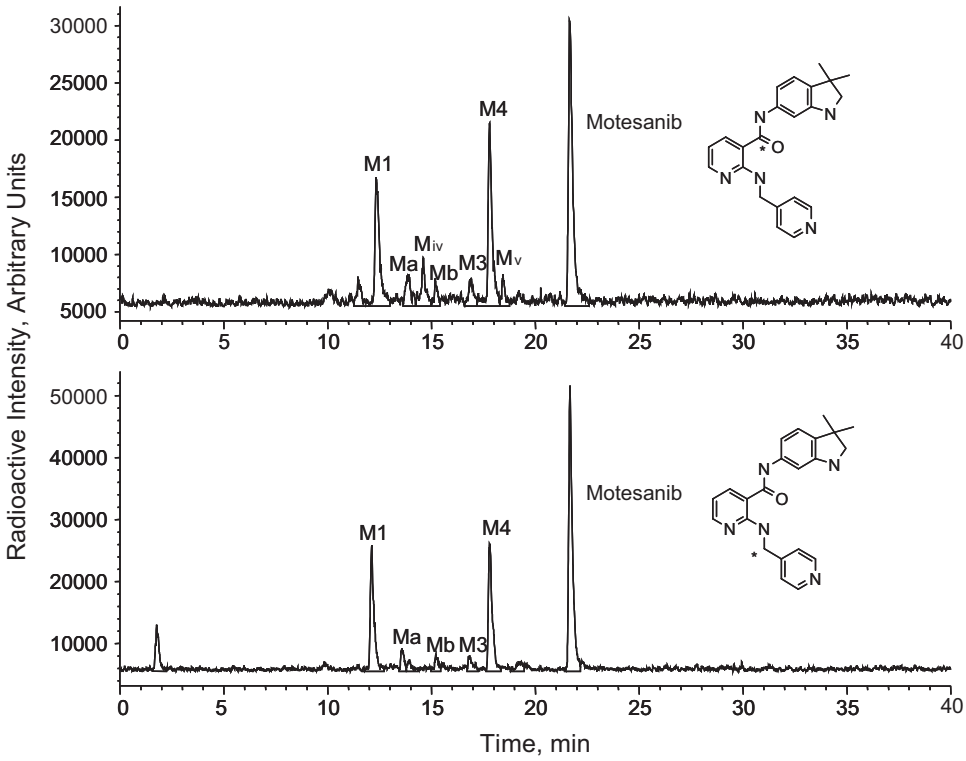

FIG. 11. In vitro metabolism profiles of motesanib in rat hepatocytes and comparison between two different ^{14}C labels of motesanib (denoted by * in the structures).

spectrometer, exact mass measurement confirmed the identity of Mx to be isonicotinic acid. The exact mass of $[M+H]^+$ of Mx was detected at *m/z* 124.0395 (−3.2 ppm from the theoretical mass of protonated isonicotinic acid, $C_6H_5NO_2$ 124.0399). The synthetic standard of isonicotinic acid showed a similar retention time and mass spectrum, thus confirming that Mx and isonicotinic acid are the same.

Oxidative Metabolism of Motesanib by Recombinant P450 Isoforms. In an NADPH-dependent manner, motesanib was metabolized by human liver microsomes into 3 major metabolites: M3 (*N*-oxide), M4 (lactam), and M5 (carbinolamine). Identification of the P450 isozymes responsible for oxidative metabolism of motesanib was performed using a combination of approaches, including metabolism by recombinant P450 isozymes and the use of P450 inhibitors and specific anti-P450 antibodies.

Motesanib (10 μM) was incubated with recombinant human P450s. Of the recombinantly expressed isoforms tested, CYP1A1, CYP2B6, CYP2D6, CYP3A4, CYP3A5, and CYP3A7 were capable of metabolizing motesanib. CYP2D6 was capable of forming M3 (*N*-oxide), M4 (lactam), and M5 (carbinolamine) in vitro, whereas CYP1A1 and CYP3A only formed lactam (M4) and carbinolamine M5 metabolite. CYP2B6 formed only the *N*-oxide M3 metabolite. The rates of formation of these oxidative metabolites by recombinant human P450s are summarized in Fig. 12.

Inhibition of Motesanib Oxidative Metabolism by Selective P450 Inhibitors. The results of experiments using specific P450 inhibitors to prevent the formation of motesanib metabolites are summarized in Fig. 13. Incubation with ketoconazole, quinidine, 8-methoxypsoralen, sulfaphenazole, and furafylline resulted in less than approximately 20% inhibition of M3 formation. The formation of M4 (lactam) and M5 (carbinolamine) metabolites of motesanib were both markedly inhibited in the presence of the CYP3A4 inhibitor, ketoconazole. Ketoconazole resulted in approximately 50% metabolic inhibition at a 1-μM concentration and approximately 70% inhibition at a 5-μM concentration. The formation of M4 was only moderately inhibited (<20%) by quinidine (CYP2D6), sulfaphenazole (CYP2C9), lansoprazole (CYP2C19), and 8-methoxypsoralen (CYP2A6). The formation of M5 was moderately inhibited (<20%) by quinidine (CYP2D6) and sulfaphenazole (CYP2C9). Results from positive control experiments confirmed that the incubations were performed under optimum conditions (Ono et al., 1996).

Inhibition of Motesanib Oxidative Metabolism by Specific Anti-P450 Antibodies. The results of anti-P450 antibody inhibition of motesanib oxidative metabolism are shown in Fig. 14. At the concentration of 10 μg/0.1 mg HLM, anti-CYP3A4 markedly inhibited formation of metabolites M4 and M5, similar to results from experiments that used specific P450 inhibitors. The formation of metabolite M3 was inhibited by approximately 50% compared with the control using the anti-CYP1A antibody. The anti-CYP2D6 antibody displayed a modest ability to prevent the formation of motesanib metabolites. Inhibition studies with human liver microsomes in the presence of CYP3A4-, CYP2D6-, and CYP1A-specific antibodies showed that CYP3A4 was the major P450 isoform responsible for the formation of the M4 and M5 metabolites; CYP2D6 and CYP1A may play a minor role in metabolism.

Motesanib *N*-Glucuronidation by Recombinant UGT Isoforms. Motesanib (10 μM) was incubated with microsomes expressing human UGTs. UGT1A4 and UGT1A1 were capable of catalyzing the *N*-glucuronidation of motesanib, with UGT1A4 exhibiting greater catalytic activity. The rates of *N*-glucuronide metabolite formation by UGT1A4 and UGT1A1 were 88.1 and 8.9 pmol/mg protein per minute, respectively. No other recombinantly expressed isoforms tested formed *N*-glucuronide metabolite (M1).

Inhibition of Motesanib *N*-Glucuronidation by Selective UGT Substrates/Inhibitors. The effect of the UGT1A1 and UGT1A4 substrates bilirubin and imipramine on *N*-glucuronidation of motesanib was tested in human liver microsomes. The results indicate that imipramine inhibited M1 formation by 64% at 1 mM and by 100% at 5 mM. Bilirubin, a specific substrate of UGT1A1, exhibited 49% inhibition at 25 μM but caused only 58% inhibition at 50 μM. However, bilirubin at higher concentrations is also known to inhibit

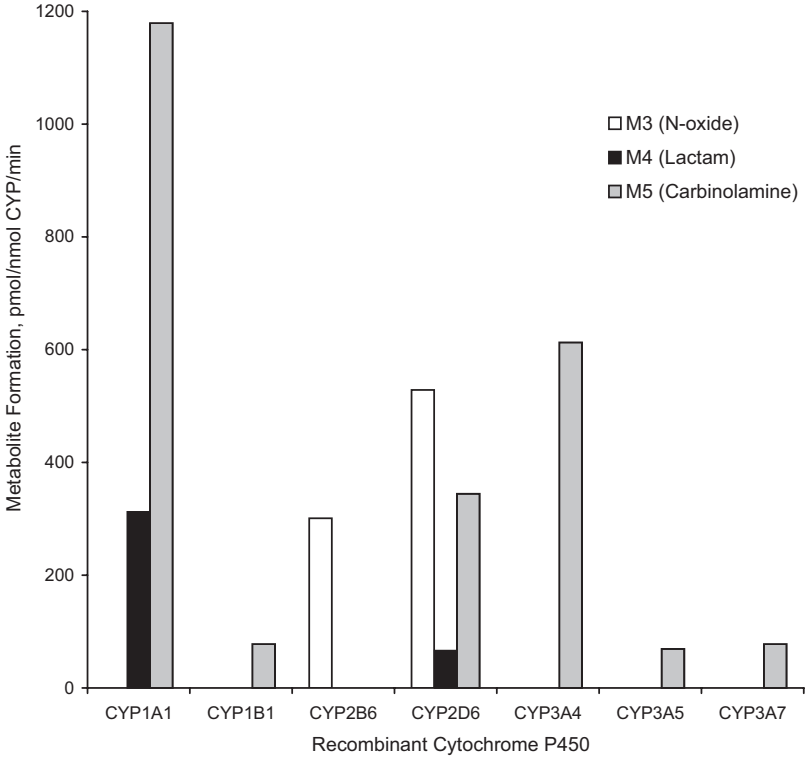

FIG. 12. Formation of oxidative metabolites of motesanib by recombinant human cytochrome P450.

UGT1A4 activity (Ghosal et al., 2004). Together, these inhibition data are in agreement with UGT isoform activity and demonstrate that UGT1A4 plays a major role in the formation of M1, whereas UGT1A1 is less important for M1 formation.

Enzyme Kinetics of Motesanib *N*-Glucuronidation in Microsomes. The enzyme kinetics of motesanib *N*-glucuronidation in human, rat, dog, and monkey liver microsomes are shown in Table 6. Human liver microsomes showed the highest efficiency for motesanib *N*-glucuronidation, with an intrinsic clearance (V_{max}/K_m) of 49.4 μl/min/mg protein. Rat, dog, and monkey liver microsomes showed a much lower intrinsic clearance of 7.8, 5.0, and 4.2 μl/min/mg protein, respectively.

Discussion

The in vitro metabolism of motesanib—a novel, highly selective oral inhibitor of VEGF receptors 1, 2, and 3, PDGF receptor, and Kit—was investigated using liver microsomes and hepatocytes from human and preclinical species. Motesanib undergoes NADPH-dependent oxidation and oxidative metabolism in human liver microsomes similar to nonhuman species. The major oxidative metabolites of motesanib were identified as *N*-oxide (M3), indoline lactam (M4), indoline carbinolamine (M5), and *N*-dealkylated metabolite isonicotinic acid (Mx).

Identification of motesanib metabolites was first based on full-scan and LC/MS/MS data. The high sensitivity, selectivity, and speed of the LC/MS technique have made it an extremely useful tool for the identification of metabolites both in vitro and in vivo (Clarke et al., 2001; Nassar and Talaat, 2004; Ma et al., 2006). With "soft" atmospheric pressure ionization techniques (either ESI or atmospheric pressure chemical ionization), most xenobiotics and their metabolites produce protonated $[M+H]^+$ and deprotonated $[M-H]^-$ molecules in positive and negative ionization modes, respectively. Molecular weight and type of biotransformation can be readily identified. With LC/MS/MS data, CID fragment patterns of the metabolites can be compared with that of the parent drug, and sites and types of biotransformation can often be pinpointed to specific substructures (Levsen et al., 2005). However, there are limitations of LC/MS data for metabolite structure assignments. For example, in the present report, the carbinolamine metabolite M5 was quite labile, and full-scan ESI produced a dehydrated ion rather than the intact protonated molecule. NMR data provided definitive structural confirmation of metabolite M5, and these data were also essential for the full structural characterization of the *N*-oxide (M3) and lactam (M4) metabolites.

Carbinolamines of aliphatic amines are generally unstable and rapidly undergo nonenzymatic dissociation resulting in *N*-dealkylation (Rose and Castagnoli, 1983). However, the carbinolamines of the *N*-heterocyclic class of compounds are more stable, and their detection and isolation have been reported previously (Murphy, 1973; Streeper et al., 1997; Vickers and Polsky, 2000; Cui et al., 2004). The carbinolamine M5 metabolite of motesanib was sufficiently stable to allow isolation, purification, and characterization by NMR. M5 was a major oxidative metabolite of motesanib in microsomes and was detected in the human and preclinical species tested. From reaction phenotyping experiments using recombinant human P450s, selective chemical inhibitors, and specific P450 inhibitory antibodies, CYP3A4 was found to be the major P450 isozyme responsible for M5 formation, with possible minor contributions from CYP2D6, CYP2C9, and CYP1A1. Approximately 70% of M5 formation was inhibited by ketoconazole and the anti-CYP3A4 monoclonal antibody.

Further oxidation of carbinolamine M5 can lead to formation of the M4 lactam metabolite. In human liver microsomes, both the CYP3A4 inhibitor ketoconazole and the CYP3A4-specific antibody inhibited M4 formation by 70%, a trend similar to their inhibition of M5 formation. CYP1A1, CYP2D6, CYP2C9, CYP2C19, and CYP2A6 seem to play minor roles in regulating the formation of M4. P450-phenotyping experiments indicated the involvement of CYP2D6 and CYP1A in the formation of the pyridyl *N*-oxide metabolite M3. The involvement of flavin-containing mono-oxygenases in M3 formation was not examined in this study and cannot be ruled out.

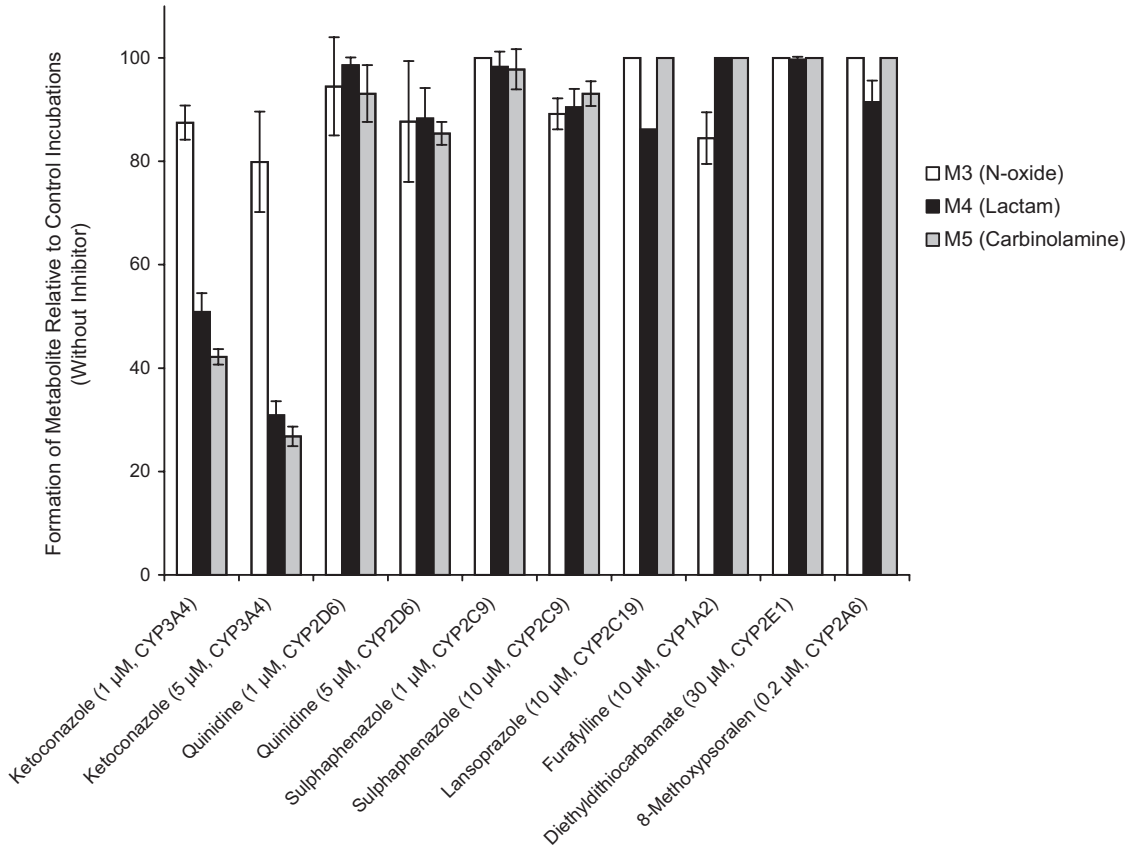

FIG. 13. Effect of isoform-selective cytochrome P450 inhibitors on the oxidative metabolism of motesanib by human liver microsomes. In positive control experiments using specific P450 inhibitors against known substrate reactions, 1 and 5 μM ketoconazole inhibited 1′-OH midazolam formation from midazolam (5 μM, with 0.1 mg/ml HLM, 5 min) by 93.1 and 98.1%; 1 and 5 μM quinidine inhibited 1′-OH bufuralol formation from bufuralol (15 μM, 0.25 mg/ml HLM, 10 min) by 77.0 and 85.3%; 1 and 10 μM sulfaphenazole inhibited 4′-OH diclofenac formation from diclofenac (5 μM, with 0.1 mg/ml HLM, 10 min) by 70.9 and 95.5%; 10 μM lansoprazole inhibited 4′-OH mephenytoin formation from *S*-mephenytoin (50 μM, with 0.5 mg/ml HLM, 30 min) by 86.5%; 10 μM furafylline inhibited acetaminophen formation from phenacetin (50 μM with 0.5 mg/ml HLM, 20 min) by 86.9%; 30 μM diethyldithiocarbamate inhibited 6-OH chlorzoxazone formation from chlorzoxazone (30 μM with 0.5 mg/ml HLM, 20 min) by 73.3%; and 0.2 μM 8-methoxypsoralen inhibited 7-OH coumarin formation from coumarin (2 μM with 0.2 mg/ml HLM, 10 min) by 94.1%.

In hepatocyte incubations, motesanib was extensively metabolized and species differences in metabolism were observed. A summary of the in vitro biotransformation of motesanib in preclinical species and in humans is shown in Fig. 15. Conjugated metabolites seemed to dominate in hepatocytes, especially in humans, with the indoline *N*-glucuronide M1 as the major metabolite (accounting for >90% of total metabolism). M1 was also detected in rat, mouse, dog, and monkey hepatocytes. Using liver microsomes and UDP-GA as a

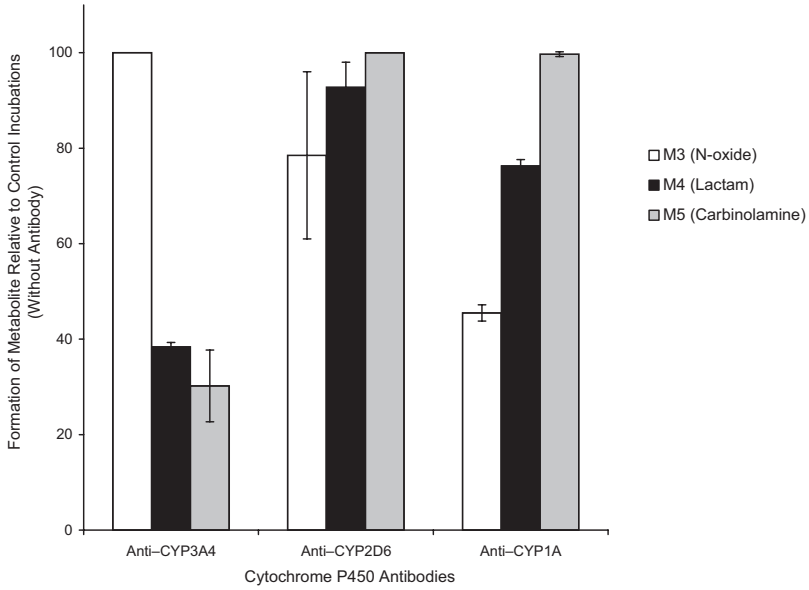

FIG. 14. Effect of isoform-selective cytochrome P450 antibodies (10 μg/0.1 mg human liver microsomes) on the oxidative metabolism of motesanib by human liver microsomes. In positive control experiments using anti-P450 antibodies (10 μg/0.1 mg of HLM) against known substrate reactions, CYP3A4 antibody inhibited 1′-OH midazolam formation from midazolam (5 μM) by 41.3%; CYP2D6 antibody inhibited 1′-OH bufuralol formation from bufuralol (15 μM) by 76.2%; and CYP1A antibody inhibited acetaminophen formation from phenacetin (50 μM) by 90.5%.

TABLE 6

Enzyme kinetics of motesanib N-glucuronidation in human, rat, dog, and monkey liver microsomes

Species	V_{max}	K_m	CL_{int}
	pmol/min/mg protein	*μM*	*μl/min/mg protein*
Human	1463	29.6	49.4
Monkey	281	67.2	4.2
Dog	795	159.0	5.0
Rat	346	44.6	7.8

CL_{int}, intrinsic clearance.

cofactor, M1 was produced in all species, but its formation was most efficient in humans. This observation is consistent with reports that species differences for *N*-glucuronidation seemed to be predominantly quantitative in nature for primary and secondary amine forming nonquaternary *N*-glucuronides (Chiu and Huskey, 1998). M1 was isolated and purified from scaled-up incubations of motesanib with human liver microsomes and UDP-GA, and its structure was fully characterized by LC/MS and NMR. M1 was very labile and susceptible to cleavage back to motesanib and glucuronic acid under very mild acidic conditions, which is consistent with reports for other unstable and acid labile primary and secondary amine *N*-glucuronides (Babu et al., 1992; Green and Tephly, 1998). In general, glucuronidation is considered a key pathway for detoxifying and eliminating drugs; thus, it is important to more fully understand the mechanism of *N*-glucuronidation, the enzymes involved, and their regulation. Our results indicate that in humans, motesanib indoline *N*-glucuronidation is catalyzed mainly by human UGT1A4 and to a lesser extent by UGT1A1.

In addition to indoline *N*-glucuronide metabolite M1, three other unusual conjugates at the alicyclic nitrogen were observed in the

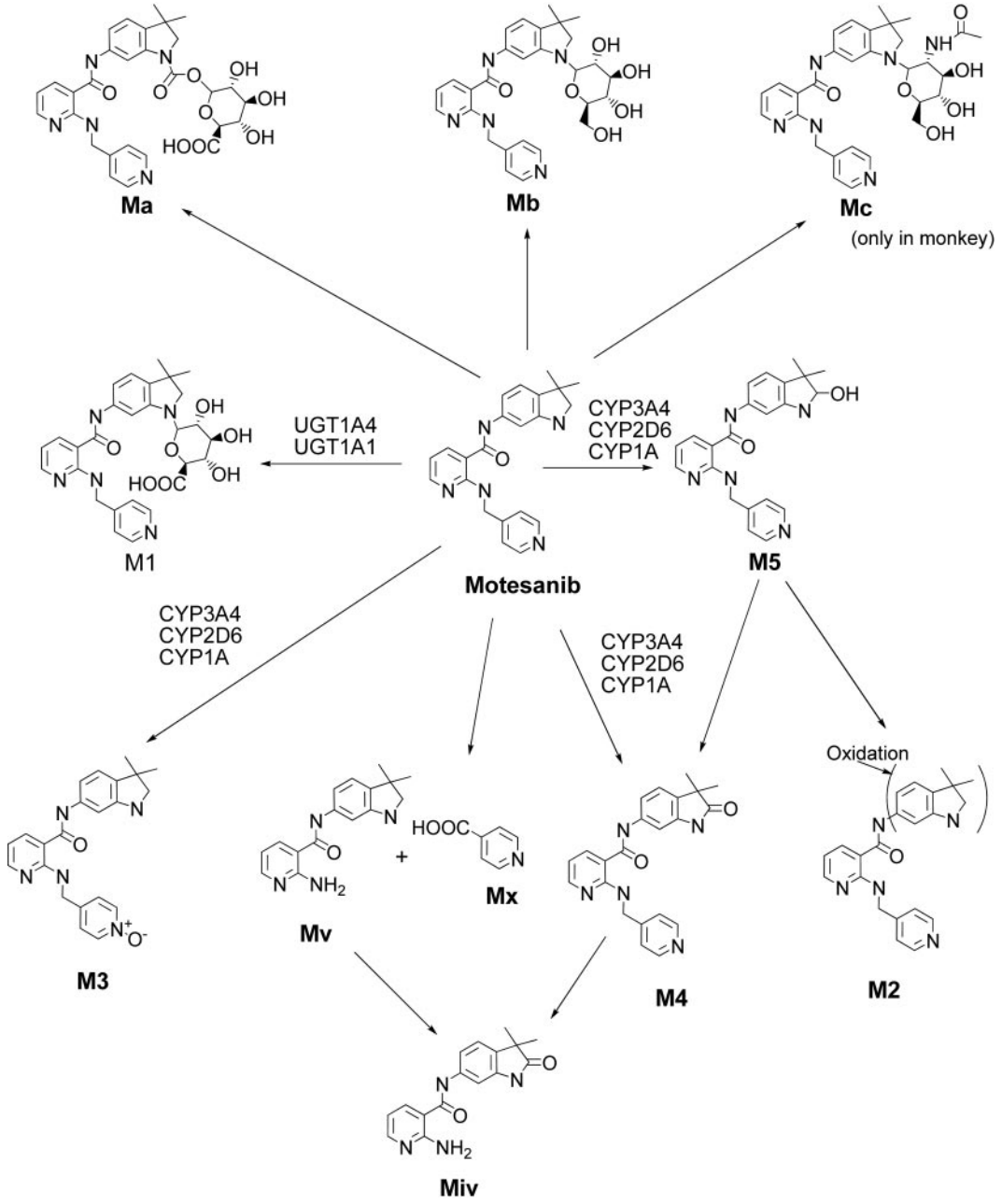

FIG. 15. Summary of in vitro metabolic pathways of motesanib.

hepatocyte incubations of motesanib. The first, Ma, an *N*-carbamoyl glucuronide metabolite found in all species except humans, was presumably formed by reaction of the amine with dissolved CO_2 to form a transient carbamic acid intermediate, followed by subsequent conjugation with glucuronic acid. *N*-carbamoyl glucuronidation is an uncommon metabolic reaction but has been reported for several primary and secondary amines, including tocainide (Elvin et al., 1980), carvedilol (Schaefer, 1992), a dipeptidyl peptidase IV inhibitor ILT-threo (Beconi et al., 2003), and sertraline (Obach et al., 2005). In vitro formation of *N*-carbamoyl glucuronide metabolites have also been reported in liver microsomes incubated in a CO_2-rich atmosphere and in carbonate buffer in the presence of UDP-GA. Obach et al. (2005) have also reported that sertraline *N*-carbamoyl glucuronidation was primarily formed by UGT2B7.

Metabolite Mb, an *N*-glucoside conjugate and second unusual conjugate at the acyclic nitrogen, was detected in hepatocyte incubations of motesanib in all preclinical species but not in human hepatocytes. The UGTs catalyze the conjugation of a variety of substrates with a sugar using UDP-sugar (UDP-GA, UDP-galactose, UDP-glucose, or UDP-xylose) as the sugar donor. *N*-Glucuronidation is a quite common and important phase II reaction for amine-containing compounds. However, *N*-glucosidation is known to be a metabolic reaction only for a limited number of compounds, including barbiturates (Tang, 1990; Toide et al., 2004) and varenicline (Obach et al., 2006). The formation of *N*-glucoside metabolite Mb in microsomal incubations derived from rat, mouse, dog, and monkey with UDP-glucose as a cofactor is consistent with results obtained using hepatocytes. The structural requirements for glucoside formation are unknown; however, they seem to share a requirement for glucuronides, and glucosidation is typically a minor pathway where glucuronidation is possible (Tang, 1990).

Metabolite Mc (*N*-acetylglucosamine conjugate), a third unusual conjugate at the acyclic nitrogen, was detected only in monkey hepatocyte incubations. Although *N*-acetylglucosaminidation has been reported as a selective conjugation reaction for ursodeoxycholic acid (Marschall et al., 1994) via *O*-linkage, formation of *N*-linked β-*N*-acetylglucosamine is extremely rare. In one report, an *N*-linked β-*N*-acetylglucosamine metabolite for the HIV-1 reverse-transcriptase inhibitor delavirdine was identified in monkey urine (Chang et al., 1997). Using UDP-*N*-acetylglucosamine as a cofactor, we observed that the metabolite Mc was produced exclusively in monkey liver microsomes.

This study is the first systematic investigation of the in vitro metabolism of motesanib, a novel, highly selective oral kinase inhibitor for the treatment of solid tumors. In human hepatocytes, motesanib undergoes extensive indoline *N*-glucuronidation (>90% of total metabolism) and to a much lesser extent, oxidative metabolism (<10%). Motesanib metabolites detected from human samples in vitro were also present in samples from rats, dogs, and monkeys, and no unique human metabolites were found. These in vitro metabolism studies and the examination of species differences in metabolism are critical for selecting the appropriate species for safety studies and for identifying the metabolites that may potentially be active or toxic, especially in light of recent U.S. Food and Drug Administration guidance on safety testing of metabolites. Predicting human in vivo metabolites and ensuring sufficient coverage of metabolites in appropriate preclinical safety studies are important for successful drug development. Follow-up absorption, distribution, metabolism, and excretion studies with radiolabeled motesanib in rats and dogs indicated very good correlation between in vitro and in vivo metabolic profiles (Amgen Inc., data on file) and will be the subject of a separate publication. The in vitro data accurately predicted the in vivo metabolic profile of motesanib and indicate that the metabolism of motesanib occurs via multiple oxidative and conjugative pathways. Furthermore, multiple P450 isozymes (CYP3A4, CYP2D6, and CYP1A1) and UGT isozymes (UGT1A4 and UGT1A1) are involved in the biotransformation of motesanib, thereby reducing the likelihood of potential drug interactions from other coadministered xenobiotics.

Acknowledgments. We acknowledge the Amgen Chemical Research and Development group for the discovery and synthesis of motesanib. We also acknowledge Dr. Tony Polverino and the Amgen Cancer Biology and Pharmacology teams for contributions to the discovery of motesanib. We thank Drs. Tom Sun and Gary Skiles (Amgen Pharmacokinetics and Drug Metabolism Department) for input and critical comments. We also thank Dr. Benjamin Scott (Complete Healthcare Communications, Inc.), whose work was funded by Amgen Inc., for expert assistance in editing this manuscript, and Dr. Beate Quednau (Amgen Medical Writing Department) for assistance in the editing process.

References

Babu SR, Lakshmi VM, Hsu FF, Zenser TV, and Davis BB (1992) Role of N-glucuronidation in benzidine-induced bladder cancer in dog. *Carcinogenesis* **13:**1235–1240.

Baillie TA, Cayen MN, Fouda H, Gerson RJ, Green JD, Grossman SJ, Klunk LJ, LeBlanc B, Perkins DG, and Shipley LA (2002) Drug metabolites in safety testing. *Toxicol Appl Pharmacol* **182:**188–196.

Beconi MG, Mao A, Liu DQ, Kochansky C, Pereira T, Raab C, Pearson P, and Lee Chiu SH (2003) Metabolism and pharmacokinetics of a dipeptidyl peptidase IV inhibitor in rats, dogs, and monkeys with selective carbamoyl glucuronidation of the primary amine in dogs. *Drug Metab Dispos* **31:**1269–1277.

Chang M, Sood VK, Kloosterman DA, Hauer MJ, Fagerness PE, Sanders PE, and Vrbanac JJ (1997) Identification of the metabolites of the HIV-1 reverse transcriptase inhibitor delavirdine in monkeys. *Drug Metab Dispos* **25:**814–827.

Chiu SH and Huskey SW (1998) Species differences in N-glucuronidation. *Drug Metab Dispos* **26:**838–847.

Clarke NJ, Rindgen D, Korfmacher WA, and Cox KA (2001) Systematic LC/MS metabolite identification in drug discovery. *Anal Chem* **73:**430A–439A.

Cui D, Subramanian R, Shou M, Yu X, Wallace MA, Braun MP, Arison BH, Yergey JA, and Prueksaritanont T (2004) In vitro and in vivo metabolism of a potent and selective integrin $\alpha_v\beta_3$ antagonist in rats, dogs, and monkeys. *Drug Metab Dispos* **32:**848–861.

Dvorak HF (2002) Vascular permeability factor/vascular endothelial growth factor: a critical cytokine in tumor angiogenesis and a potential target for diagnosis and therapy. *J Clin Oncol* **20:**4368–4380.

Elvin AT, Keenaghan JB, Byrnes EW, Tenthorey PA, McMaster PD, Takman BH, Lalka D, Manion CV, Baer DT, Wolshin EM, et al. (1980) Tocainide conjugation in humans: novel biotransformation pathway for a primary amine. *J Pharm Sci* **69:**47–49.

Ghosal A, Hapangama N, Yuan Y, Achanfuo-Yeboah J, Iannucci R, Chowdhury S, Alton K, Patrick JE, and Zbaida S (2004) Identification of human UDP-glucuronosyltransferase enzyme(s) responsible for the glucuronidation of posaconazole (Noxafil). *Drug Metab Dispos* **32:**267–271.

Green MD and Tephly TR (1998) Glucuronidation of amine substrates by purified and expressed UDP-glucuronosyltransferase proteins. *Drug Metab Dispos* **26:**860–867.

Hastings KL, El-Hage J, Jacobs A, Leighton J, Morse D, and Osterberg RE (2003) Drug metabolites in safety testing. *Toxicol Appl Pharmacol* **190:**91–92; author reply 93–94.

Heinrich MC, Blanke CD, Druker BJ, and Corless CL (2002) Inhibition of KIT tyrosine kinase activity: a novel molecular approach to the treatment of KIT-positive malignancies. *J Clin Oncol* **20:**1692–1703.

Levsen K, Schiebel HM, Behnke B, Dötzer R, Dreher W, Elend M, and Thiele H (2005) Structure elucidation of phase II metabolites by tandem mass spectrometry: an overview. *J Chromatogr A* **1067:**55–72.

Ma S, Chowdhury SK, and Alton KB (2006) Application of mass spectrometry for metabolite identification. *Curr Drug Metab* **7:**503–523.

Marschall HU, Griffiths WJ, Zhang J, Wietholtz H, Matern H, Matern S, and Sjövall J (1994) Positions of conjugation of bile acids with glucose and N-acetylglucosamine in vitro. *J Lipid Res* **35:**1599–1610.

Murphy PJ (1973) Enzymatic oxidation of nicotine to nicotine 1′(5′) iminium ion. A newly discovered intermediate in the metabolism of nicotine. *J Biol Chem* **248:**2796–2800.

Nassar AE and Talaat RE (2004) Strategies for dealing with metabolite elucidation in drug discovery and development. *Drug Discov Today* **9:**317–327.

Obach RS, Cox LM, and Tremaine LM (2005) Sertraline is metabolized by multiple cytochrome P450 enzymes, monoamine oxidases, and glucuronyl transferases in human: an in vitro study. *Drug Metab Dispos* **33:**262–270.

Obach RS, Reed-Hagen AE, Krueger SS, Obach BJ, O'Connell TN, Zandi KS, Miller S, and Coe JW (2006) Metabolism and disposition of varenicline, a selective $\alpha4\beta2$ acetylcholine receptor partial agonist, in vivo and in vitro. *Drug Metab Dispos* **34:**121–130.

Ono S, Hatanaka T, Hotta H, Satoh T, Gonzalez FJ, and Tsutsui M (1996) Specificity of substrate and inhibitor probes for cytochrome P450s: evaluation of in vitro metabolism using cDNA-expressed human P450s and human liver microsomes. *Xenobiotica* **26:**681–693.

Polverino A, Coxon A, Starnes C, Diaz Z, DeMelfi T, Wang L, Bready J, Estrada J, Cattley R, Kaufman S, et al. (2006) AMG 706, an oral, multikinase inhibitor that selectively targets vascular endothelial growth factor, platelet-derived growth factor, and Kit receptors, potently inhibits angiogenesis and induces regression in tumor xenografts. *Cancer Res* **66:**8715–8721.

Rose J and Castagnoli N Jr (1983) The metabolism of tertiary amines. *Med Res Rev* **3:**73–88.

Rosen LS, Kurzrock R, Mulay M, Van Vugt A, Purdom M, Ng C, Silverman J, Koutsoukos A, Sun YN, Bass MB, et al. (2007) Safety, pharmacokinetics, and efficacy of AMG 706, an oral multikinase inhibitor, in patients with advanced solid tumors. *J Clin Oncol* **25:**2369–2376.

Schaefer WH (1992) Formation of a carbamoyl glucuronide conjugate of carvedilol in vitro using dog and rat liver microsomes. *Drug Metab Dispos* **20:**130–133.

Song S, Ewald AJ, Stallcup W, Werb Z, and Bergers G (2005) PDGFRbeta+ perivascular progenitor cells in tumours regulate pericyte differentiation and vascular survival. *Nat Cell Biol* **7:**870–879.

Streeper RT, Pearson PG, Zhao Z, Mizsak SA, Sanders PE, Wienkers LC, and Vrbanac JJ (1997) In vitro metabolic transformations of 2,4-dipyrrolidinylpyrimidine: a chemical probe for P450-mediated oxidation of tirilazad mesylate. *Xenobiotica* **27:**1131–1145.

Tang BK (1990) Drug glucosidation. *Pharmacol Ther* **46:**53–56.

Toide K, Terauchi Y, Fujii T, Yamazaki H, and Kamataki T (2004) Uridine diphosphate sugar-selective conjugation of an aldose reductase inhibitor (AS-3201) by UDP-glucuronosyltransferase 2B subfamily in human liver microsomes. *Biochem Pharmacol* **67:**1269–1278.

Vickers S and Polsky SL (2000) The biotransformation of nitrogen containing xenobiotics to lactams. *Curr Drug Metab* **1:**357–389.

Address correspondence to: Dean Hickman, Department of Pharmacokinetics and Drug Metabolism, Mail Stop 30E-2-B, Amgen Inc., One Amgen Center Dr., Thousand Oaks, CA 91320-1799. E-mail: deanh@amgen.com